2023

Acausal Modeling of Wind Turbines with Validation and Control Studies

Kazi Ishtiak Mohsin
University of Central Florida

ACAUSAL MODELING OF WIND TURBINES WITH VALIDATION AND CONTROL STUDIES

by

KAZI ISHTIAK MOHSIN
B.Sc. Bangladesh University of Engineering and Technology, 2017

A thesis submitted in partial fulfilment of the requirements
for the degree of Master of Science
in the Department of Mechanical and Aerospace Engineering
in the College of Engineering and Computer Science
at the University of Central Florida
Orlando, Florida

Fall Term
2023

Major Professor: Tuhin Das

ABSTRACT

This thesis involves the modeling, validation, and control studies of a Control-Oriented, Reconfigurable, and Acausal Floating Turbine Simulator (CRAFTS), that is currently under development. CRAFTS uses Modelica®, an object-oriented, declarative, multi-domain modeling language for physical system modeling in the Dymola environment. The CRAFTS simulator facilitates rapid dynamic simulation of wind turbines with various model variants and enables control co-design.

A major emphasis of this thesis is in the validation of the CRAFTS simulator for a 15-MW land-based wind turbine through several test cases. These test cases were collaboratively developed in conjunction with other participating research entities. CRAFTS has undergone rigorous testing, with a particular emphasis on comparison against the industry standard OpenFAST platform (developed by the National Renewable Energy Lab (NREL)) as well as experimental data. Open loop testing scenarios scrutinize the wind turbine dynamic conditions such as varying rotor speed and pitching angle maneuvers. Diverse combinations of ramp and step commands have been employed to modulate rotor speeds and pitching angles. Validation results indicate very good agreement between CRAFTS and baseline results.

CRAFTS was also tested under various types of closed-loop control scenarios, such as different types of wind profiles and various wind velocities. Wind types encompass stepped winds, wind gusts, steady winds, and sinusoidal wind patterns. In closed loop testing, firstly an industry standard controller ROSCO (also developed by NREL) was used. Thereafter, a nonlinear controller developed in our prior research was implemented and investigated. The closed loop performance of the CRAFTS model was compared with OpenFAST. The tests confirmed the validity of the CRAFTS model under closed-loop and also validated the nonlinear controller.

The work was a critical element in the development of the CRAFTS simulator. Validation tests

provided valuable insight into the accuracy of the underlying physics and often provided valuable feedback that led to model improvements. The work has laid the foundations for more advanced research, especially in the area of multivariable control design for floating offshore wind turbines.

I dedicate this work to my parents, my supervisors and all my well wishers

ACKNOWLEDGMENTS

I would like to express my sincere gratitude to my advisor, Dr. Tuhin Das for granting me the opportunity to work on such an interesting research area and for always being supportive throughout my academic journey. Without his continuous support and guidance, my journey to this point would have never been possible. I am equally grateful to my co-advisor, Post-Doctoral Scholar Dr. Tri D. Ngo, for his consistent and invaluable guidance. His mentorship has not only provided me with the necessary tools to immerse myself in research but has also significantly contributed to the success of my research endeavors. I am thankful for the assistance of my colleagues at the Hybrid Sustainable Energy Systems Laboratory (HYSES), whose collaborative spirit has been instrumental in my progress. I would like to extend my appreciation to the members of my thesis committee, Dr. Yunjun Xu, and Dr. Jeffrey Kauffman, for their interest in my work

TABLE OF CONTENTS

LIST OF FIGURES

LIST OF TABLES

CHAPTER 1: INTRODUCTION

Over the past decade, the domain of wind energy has witnessed a pronounced escalation in research and developmental endeavors. In 2021, the United States achieved a remarkable milestone in wind energy, installing 13,413 MW of new capacity, bringing the cumulative total to 135,886 MW, and representing a $20 billion investment. Wind power now accounts for over 9% of the nation's electricity generation, with select states like Iowa and South Dakota surpassing the 50% mark in wind energy utilization. This impressive growth is propelled by technological advancements and policy support, notably the Production Tax Credit, with newly installed wind turbines averaging 3 MW in capacity, reflecting a 9% increase from the previous year [1].

Moreover, the comprehensive advantages of wind energy, encompassing health, climate benefits, and grid system enhancements, far exceed its levelized cost of energy, dropping notably from 0.089 USD/kWh to 0.039 USD/kWh for onshore wind and from 0.162 USD/kWh to 0.084 USD/kWh for offshore wind, marking a percentage reduction of 56% and 48%, respectively [2]. Notably, offshore wind energy in the United States garnered substantial momentum, with a 14% increase in the offshore wind project pipeline within a single year, now encompassing 40,083 MW in various developmental stages, including two operational projects totaling 42 MW. The Bureau of Ocean Energy Management played a pivotal role in expanding this pipeline through lease auctions and conversions in critical regions like the Atlantic and California. Globally, the offshore wind sector witnessed a groundbreaking year in 2021, achieving installations of 17,398 MW, elevating the cumulative installed capacity to 50,623 MW across 257 projects. Turbine sizes continued to grow, with rotor diameters averaging 156 meters and turbine capacities surpassing 7 MW. Furthermore, the worldwide pipeline for floating offshore wind energy has more than doubled in 2021, reaching an impressive 60,746 MW. These developments underscore the dynamic and auspicious landscape of wind energy, both within the United States and on a global scale, reaffirming its pivotal role in

the transition toward sustainable and clean energy sources.

The recent surge in interest has led to a multitude of research studies and publications investigating the effectiveness and dependability of wind turbines as a source of power generation. However, due to the growing size of these turbines and the associated expenses, it is often impractical to construct and operate a full-scale wind turbine for the purpose of evaluating its performance and power generation capacity. The situation becomes even more challenging in the case of floating wind turbines, as it introduces an extra layer of uncertainty associated with both wave dynamics and wind dynamics. To overcome these challenges and to optimize and extract as much power as possible from wind turbines, researchers have opted to utilize small-scale model prototyping,

Figure 1.1: Wind turbine farm [37]

modeling, and simulation platforms to enable them to look into the dynamics of wind turbine operations and to locate areas for improvement. In such situations, it is imperative to confirm the model's accuracy by subjecting it to various test cases. This validation process ensures that the model aligns with the aerodynamic and structural performance standards, using both available experimental data and widely recognized industry software packages. In addition to the modeling of wind turbine dynamics, it holds significant importance to assess the model's suitability for control system design. Given the wind turbine's need to withstand diverse environmental conditions, including varying wind patterns and waves, it becomes essential to integrate diverse control mechanisms. This ensures the consistent generation of power and mitigates the potential adverse impact of wind and waves on various structural components, thereby extending its operational lifespan. Hence, when prototyping or modeling a wind turbine within a simulation environment, it is crucial to verify both its aerodynamic and structural precision, while also ensuring that the newly created model is suitable for designing control systems.

The requirement to concurrently develop a model, validate it, and ensure its suitability for control system design has led to the emergence of the concept known as Control Co-Design (CCD). When modeling wind turbine dynamics, it is essential to investigate the model's compatibility with CCD. CCD refers to the concept of simultaneous system development and control design in the process of developing technology. This concurrent approach facilitates design iteration, intelligent choice of sensing and actuation, and effective control design to be integrated into the technology development process. Recognizing the significance of the previously mentioned requirement, we have devised the following strategy for modeling, validation, and control system design, which serves as the central focus of this thesis. Primary objectives of this thesis along with the outline of it are described in the following paragraphs:

1.1 Thesis Objective

- In support of the ongoing advancements in floating offshore wind turbine technology, we have developed CRAFTS (Control-oriented Re-configurable Acausal Floating Turbine Simulator) in an acausal manner using Modelica language in Dymola environment. Modelica is an object-oriented, declarative, multi-domain modeling language for component-oriented modeling of complex systems. Modelica® is selected as a modeling language due to its increased composability, plug and play feature, and bi-directional information exchange. Details of Modelica® would be discussed later on. CRAFTS serves as an indispensable tool for delving into the intricacies of turbine dynamics and behavior under diverse environmental conditions. It's worth noting that a significant portion of the modeling work for CRAFTS was undertaken by my colleague, Mohammad, who made substantial contributions to this project.

- The primary focus of this thesis revolves around the testing and validation of the CRAFTS model across a spectrum of test cases. CRAFTS has undergone rigorous open-loop validation processes, including comparison against the well-established industry standard, OpenFAST [22], which was developed by NREL (National Renewable Energy Laboratory). Through a series of diverse test cases (discussed in Chapter 5), CRAFTS has been put to the test to ensure its aerodynamic and structural accuracy and reliability. Through these open-loop test cases, several areas for improvement in both aerodynamics and structural aspects were identified and subsequently integrated, resulting in enhanced performance accuracy for CRAFTS. Moreover, theoretical analysis of certain test cases have been conducted to gain a more comprehensive understanding of the aerodynamic behavior. These analyses also encompass sensitivity studies involving various aerodynamic aspects of the turbine. These investigations aim to offer critical insights essential for the design of various control systems.

- In addition to the open-loop validation of the CRAFTS model, this thesis has dedicated substantial attention to closed-loop validation. CRAFTS experienced comprehensive testing within various closed-loop scenarios, as detailed in Chapter 5, incorporating the industry-standard ROSCO controller [20] developed by NREL. The model's performance was verified against the industry-standard wind turbine software, OpenFAST, within these identical closed-loop scenarios. validation conducted in these closed-loop testing scenarios has affirmed the suitability of the CRAFTS model for control system design.

- Furthermore, CRAFTS has been subjected to a nonlinear controller developed in our prior research to showcase its versatility and adaptability in the realm of control system design. The performance of CRAFTS, when equipped with a nonlinear controller, has been subjected to validation alongside the ROSCO controller to demonstrate its accurate closed-loop response. Moreover, these open-loop and closed-loop validation results shows the reliability of CRAFTS model for the exploration and innovation of control techniques especially in the area of multivariable control aimed at enhancing turbine performance.

1.2 Thesis Outline

This thesis book has been outlined in the following manner: Chapter 2 provides a comprehensive review of existing modeling techniques employed by various researchers for wind turbine development. It also delves into a range of control techniques devised to enhance turbine performance across different sectors. Chapter 3 offers an in-depth exploration of the modeling techniques utilized in CRAFTS, providing detailed insights into its modeling approach. In Chapter 4, we shift our focus to the control modules incorporated into the CRAFTS model, shedding light on the key aspects of the control system. Chapter 5 presents the validation process of CRAFTS, encompassing a series of test cases conducted under both open-loop and closed-loop conditions. Chapter 6

introduces the implementation of a non-linear controller within the CRAFTS model and compares the results with those achieved using the ROSCO controller. The thesis concludes in Chapter 7 with a summary of findings and outlines potential avenues for future research and development in this field.

CHAPTER 2: LITERATURE REVIEW

In the development of wind turbine modeling different researchers around the world have developed various software tool to look into the dynamics of the turbine. In the casual modeling approach, OpenFAST is a multi-physics engineering tool for simulating the coupled dynamic response of wind turbines developed by NREL [22]. OpenFAST joins aerodynamics models, hydrodynamics models, servo dynamics models, and structural dynamics models to enable coupled nonlinear aero-servo-elastic simulation in the time domain. OpenFAST is constructed from a number of discipline-specific modules coupled together with glue-code in state-space [22]. The aerodynamic models use wind-inflow data and solve for the rotor-wake effects and blade-element aerodynamic loads, including dynamic stall and aeroacoustics. The control and electrical system models simulate the controller logic, sensors, and actuators of the blade-pitch, generator-torque, nacelle-yaw, and other control devices, as well as the generator and power-converter components of the electrical drive. The structural-dynamics models apply the control and electrical system reactions, apply the aerodynamic and hydrodynamic loads, add gravitational loads to model structural dynamics, to simulate the elasticity of the rotor, drivetrain, and support structure. Coupling between all models is achieved through a modular interface. In a paper authored by Lemmer et al. [4], a modeling approach for existing Floating Offshore Wind Turbine (FOWT) platforms is proposed to achieve a comprehensive understanding of the system dynamics at the concept phase. This method consists of a flexible multibody system, with a Newton–Euler algorithm independent of the multibody layout and aerodynamic and hydrodynamic models. By comparing this model to higher-fidelity models and experiments, it has been verified that even with its simplifications, the response magnitude to wind and wave forces can be accurately predicted. These simulations are fast enough to allow large sensitivity studies and multidisciplinary optimizations for systems engineering approaches.

In the acausal modeling approach, Petersson et al. [5] developed an acausal model of a vertical land-based wind turbine. In their research, they proved the feasibility of developing acausal wind turbine models using the Modelica language and the Dynamic Modeling Laboratory (*Dymola*) platform. However, their model was not validated against real measurement data as the authors did not have access to experimental/operational data. Nonetheless, the model was used to test turbine control strategies. Eberhart et al. [6] introduced an open source Modelica library named *WindPowerPlants*. This library leverages Modelica's multi-domain approach by developing a wind turbine model, a generator model, and a connection to the grid. However, the library is based on power balance, losses are neglected, and controls were largely underdeveloped. This approach would require prior knowledge of the turbine's characteristic $C_P - \lambda$ and $C_T - \lambda$ curves. While this approach to modeling, assessing, and predicting the energy output of a single wind turbine or an entire wind farm is of great use, it does not lend itself into the prototyping and development of new wind turbines as it requires prior knowledge of the turbine's performance parameters. Nonetheless, the library proved capable of predicting the energy output of existing wind turbine models with a relative power deviation prediction of $\pm 6\%$ from the reference power.

A Modelica for Wind Turbines (MoWiT) library for the multi-physics floating offshore wind turbine (FOWT) systems with the aero-hydro-servo-elastic dynamics was developed by the Fraunhofer Institute for Wind Energy Systems (IWES) [7]. For the aerodynamic modeling, MoWiT uses the blade-element momentum (BEM) theory, or the generalized dynamic wake (GDW) model, and incorporates corrections for the dynamic wake and dynamic stall (DS). Regarding hydrodynamics, the MoWiT is capable of using linear Airy or nonlinear Stokes wave theory, Wheeler stretching (WS) or delta stretching, Morison equation (ME), and MacCamy-Fuchs (MCF) approach. In MoWiT, the controller is implemented as a Dynamic Link Library (DLL) from the GH Bladed code. These controller DLLs include logic for variable-speed generator torque and collective blade pitch-to-feather control. For the structural dynamics, the finite element method (FEM), based on

Euler-Bernoulli or Timoshenko beam theory, or modal reduction can be used for the floater and turbine representation. The mooring lines are modeled through a multibody-dynamics (MBD) or mass-spring-damping (MSD) system, which considers, apart from the dynamic inertial motion of the mooring system, hydrodynamic and internal damping, elastic deformation, as well as soil contact, and uses the catenary equation for determining the initial shape and position of the mooring line elements. The FOWT performance was verified using the Offshore Code Comparison Collaboration (OC3) phase IV spar-buoy FOWT system found within the International Energy Agency (IEA) Wind Task 23, Subtask 2. Furthermore, MoWiT was also used by IWES during the OC5 phase III project verification [8] and validation [9].

In the control aspect, operating conditions of variable-speed wind turbines are usually divided into two regimes: Regime 2 where the wind speed is below the rated speed; Regime 3 where the wind speed is above the rated speed. Control in Regime 2 has been reported in literature [10, 16, 15] where maximization of the extracted power is the focus. The standard approach for maximizing the power output is to regulate the generator torque to maintain the turbine near the optimum tip-speed ratio.

In a technical report by Jonkman et al. [11], a baseline controller including a torque controller for Regime 2 and a pitch controller for Regime 3 was proposed and validated on a 5-MW reference wind turbine. In a later work, Abbas et al. [12] updated the baseline controller by implementing a thrust peak shaving feature to minimize the thrust experienced by the wind turbine. A setpoint smoother for minimizing power fluctuations when transitioning between Regime 2 and 3 was also implemented. The updated controller eases the automatic tuning process while maintaining or improving the performance of the baseline controller. In a work published by Y.D.Song et al. [40] , a non-linear adaptive control based on the regulation of excitation winding voltage of the generator have been proposed to achieve smooth and satisfactory rotor speed tracking. Moreover, wind speed estimator-based control has been used in recent days for rotor speed tracking. Having

prior knowledge of wind speed can facilitate easier tracking of rotor speed. However, incorporating an anemometer increases the overall cost, maintenance requirements, and reduces the reliability of the overall system. In a review paper conducted by Jena et al.[41] , the pros and cons of effective wind speed estimation have been discussed. Various control algorithms based on the findings of the review have been highlighted. Drawing from this review, conclusions have been drawn regarding the conditions under which wind review-based control can be effective and the potential consequences of ineffective wind speed estimation. Furthermore, machine learning and neural network-based estimation and control have been gaining popularity in various engineering sectors, including data analysis, transportation, the medical field, control systems, and so forth [38]. In a publication by Li et al. [43], a genetic algorithm-based support vector machine model is adopted to estimate wind speed, utilizing physically measurable signals such as electrical power, pitch angle, and rotor speed. Subsequently, the desired rotor speed can be obtained accordingly. Additionally, a novel neuroadaptive controller based on virtual parameters is developed by combining radial basis function neural networks with adaptive algorithms. This controller is designed to accommodate system uncertainties and mitigate external disturbances.

In addition to the regulation of rotor speed for optimal turbine performance, it holds paramount importance to mitigate the fatigue loads affecting the turbine, as these loads profoundly impact the turbine's operational lifespan. While it's important to note that this thesis does not specifically delve into fatigue load reduction, we do wish to shed light on various control algorithms that have been proposed and implemented to not only regulate rotor speed but also address the objective of minimizing fatigue loads. In a work published by Schuler et al. [13], an L1-control scheme for pitch control in Regime 3 was proposed. Two decoupled linear time-invariant models were derived to design individual and collective pitch controllers independently. Individual pitch control is deployed to reduce the bending moments experienced on the blade root, whereas collective pitch control regulates the rotor speed and further reduces blade root bending moments. Compared

to standard control schemes, this research reported a significant load reduction without losses in energy production. In Geyler et al. [14], a multi-variable pitch control design with decoupled controllers for collective and cyclic pitch control using H_∞ norm minimization approach was discussed and proposed. The controller has the objective of speed control as well as providing active tower damping since speed control and active tower damping are highly coupled. In addition to regulating speed and increasing the damping, the controller demonstrated the ability to reduce 1P fluctuations in the blade root bending moments through cyclic pitch control. The control design was verified by simulations.

In a study by Verwaal et al. [18], a controller using model predictive control and feed-forward control strategies has been verified. It surpassed the performance of a baseline controller in terms of rotor speed regulation under wind speed disturbance due to phase lead in the control input. The baseline controller used in this paper is a standard proportional-integral controller, which has the rotational speed of the rotor as an input measurement. Moreover, Laks et al. [17] proposed a pitch controller with preview-based disturbance feedforward control for load mitigation and speed regulation. Performance evaluation has shown significant load mitigation while assuming highly idealized wind measurements. However, in the case of more realistic measurements such as wind shear, controller performance is greatly diminished if further optimization of the controller and/or better processing of measurements are not considered.

To support the CCD approach, to bridge the existing aerodynamic and structural gap in various wind turbine software packages, to offer a user-friendly software package for wind turbines with a graphical format that enhances the comprehension of their physical structure and to facilitate the innovation of different control techniques to enhance the performance of the wind turbine a Control-oriented, Reconfigurable and Acausal Floating Turbine Simulator (CRAFTS) has been developed. The aim of this simulation platform is to assess and provide further insight into the dynamics and performance of wind turbines under various operational conditions and scenarios.

In addition, the model facilitates control co-design by emphasizing subsystem interactions from the very inception and formulation of the model. This adapts to design changes, and allows rapid simulations to validate models and optimize sensor, actuator placement, and control strategies. This approach and modeling effort has been facilitated by the use of the *Dymola* software built around the Modelica language, which is discussed further in Chapter 3. CRAFTS has undergone an extensive testing process, encompassing both open-loop and closed-loop scenarios, across a spectrum of operational and environmental conditions. This rigorous evaluation was conducted to affirm its accuracy concerning aerodynamics, structural integrity, and its adaptability for control system design.

It's noteworthy to mention that CRAFTS is currently in its developmental phase, which includes the incorporation of various features, notably nonlinear elements experienced during wind turbine operations. However, a substantial portion of the core functionalities has already been integrated and rigorously tested. This positioning makes it well-suited for investigating various aerodynamic phenomena and deploying control systems aimed at augmenting wind turbine performance.

The major contributions of this thesis can be summarized in the following manner:

- A Control-oriented, Re-configurable, and Acausal Floating Turbine Simulator (CRAFTS) has been developed and discussed to enable rapid and accurate simulation of wind turbines. Though this thesis discusses the modeling technique employed in CRAFTS but my main contribution in the modeling section was to troubleshoot various aerodynamic and structural blocks used during the modeling stage.

- A modular library structure with physics-based models-CRAFTS is validated against industry-standard platforms such as OpenFAST developed by NREL in several open-loop conditions under varying operating conditions. The outcomes obtained from the validation of these open-loop test cases played a pivotal role in identifying areas for improvement within CRAFTS. These improvements were subsequently integrated to achieve better aerodynamic accuracy.

- This thesis places significant emphasis on assessing the closed-loop performance of CRAFTS when coupled with ROSCO across diverse environmental conditions. Furthermore, the response of CRAFTS has been meticulously validated against the response of OpenFAST, thereby ensuring the model's ability to provide accurate closed-loop responses.

- An in-house nonlinear controller [36] has been implemented in CRAFTS which was developed in our prior research and it's performance have been tested against industry standard controller ROSCO [20] to ensure versatility of CRAFTS in control system design which would led the way for different multivariable control design using CRAFTS.

I would like to highlight that the majority of the modeling work, as discussed in item 1, was carried out by my colleague. My primary contributions were primarily in items 2, 3, & 4 with some involvement in item 1. Moreover, it's worth mentioning that CRAFTS is portable with causal

platforms such as MATLAB, and Computer-Aided Engineering (CAE) platforms for wind energy research. Validation results of CRAFTS with OpneFast and experimental data which is conducted by FOCAL EXPERIMENTAL PROGRAM (NREL) - Floating Offshore-wind and Controls Advanced Laboratory Experiment to Generate Data Set to Accelerate Innovation in Floating Wind Turbine Design and Controls have been published in the following articles [24, 25, 26, 27].

CHAPTER 3: ACAUSAL MODELING OF WIND TURBINES

In this chapter, we delve into the construction of the CRAFTS simulation environment, which relies on the Modelica language. Modelica is a multi-domain modeling language that employs an object-oriented and declarative approach for the detailed modeling of intricate systems. We explore the distinctive attributes of the Modelica language and elucidate the methodology employed in crafting the CRAFTS model, providing essential insights into its model specifications. As mentioned before majority of the modeling work has been conducted by my colleague (Mohammad). So this chapter is primarily based on his work but this chapter is essential to establish the foundation of subsequent chapters.

3.1 Features of Acausal Modeling

CRAFTS supports acausal connection of components governed by mathematical equations to facilitate modeling from first principles [28]. The choice of using Modelica as the programming platform was further encouraged by its plug-and-play interface, which allows any set of dynamical, electrical, thermal, or control processes to be interconnected in such a fashion that a desired system is constructed.

Furthermore, the object-oriented features of Modelica permits the reuse/swapping of models, allowing for simulation of multiple system configurations (e.g. swapping a three-bladed hub with a two-bladed hub) without any significant remodeling on the user's behalf. Lastly, Modelica's acausal modeling opens up a new approach to modeling due to increased composability, where composability is the ability to drag, drop, and connect components in the modeling space without worrying about causal implications. This is true because Modelica is designed with physical

information exchange rather than directional signal flow (cause and effect) in the block diagram modeling approach. The acausal modeling approach can be easily demonstrated by a spring-mass-damper model.

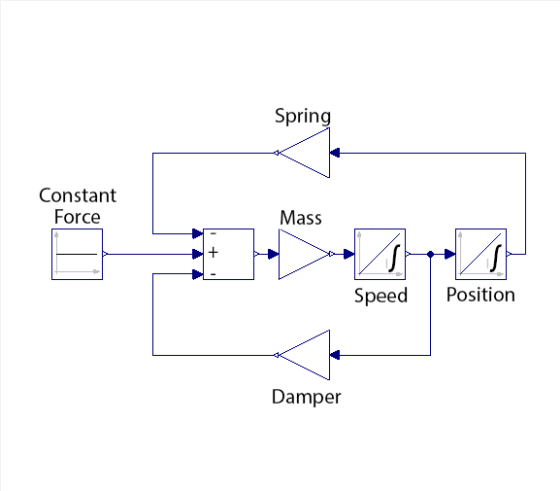

(a) Causal: Single spring-mass-damper model

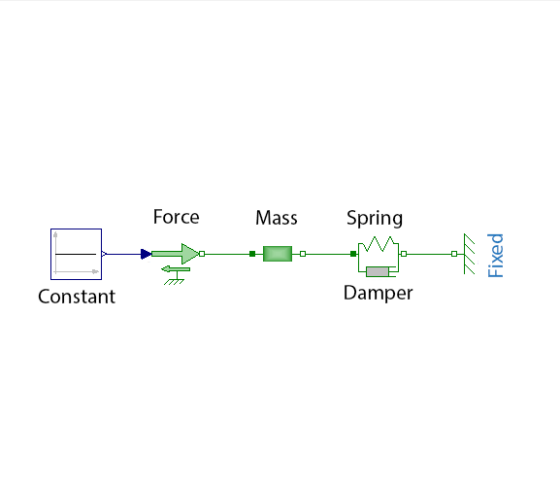

(b) Acausal: Single spring-mass-damper model

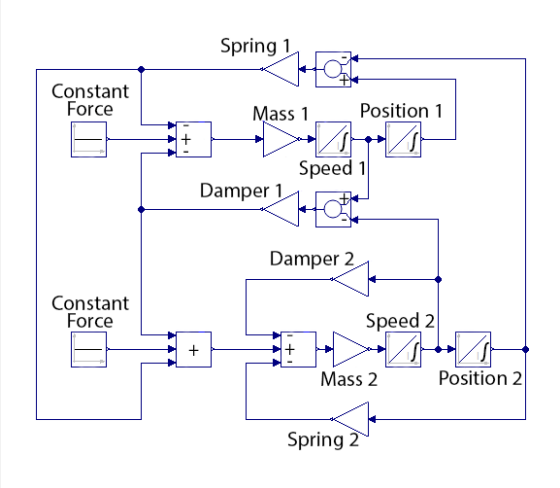

(c) Causal: Multiple spring-mass-damper model

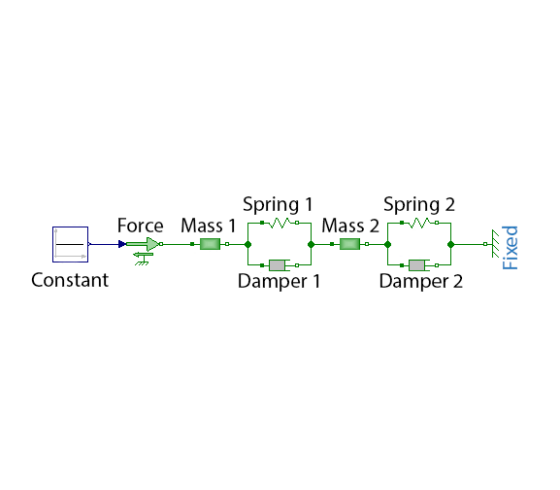

(d) Acausal: Multiple spring-mass-damper model

Figure 3.1: (a, c) Causal and (b, d) acausal implementations of a spring-mass-damper model

Take the example presented in Fig.3.1 for instance. In Fig.3.1a, the system is constructed using

conventional signal blocks with gains, integrators, and a predefined directionality for the causal signal flow. Whereas in Fig.3.1b, the system is modeled using standard Modelica components that are inherently acausal. If another set of spring-mass-damper were added in series to the previous model, the complexity of the causal model increases dramatically as depicted in Fig.3.1c and Fig.3.1d. Comparing both figures, the simplicity that the acausal approach facilitates in the modeling of the system can be appreciated. It can be seen in 3.1b, and 3.1d that component connections in acausal modeling mimic connectivity and interactions in physical systems. For more details about the demonstration of these benefits in Modelica, interested readers may consult Chapter 11 of *Introduction to Physical Modeling with Modelica* by Tiller [29]. This is a general feature of acausal modeling. On the contrary, causal approaches are more focused on programming mathematical equations.

The acausal modeling approach also facilitates the application of CCD methodologies that integrate all relevant engineering disciplines at the start of the design process with feedback control and dynamic interaction principles as the primary drivers of design. CCD methodologies enable designers to analyze the interactions of the wind turbine's aero-, hydro-, elastic-, electric-, economic-, and servo-system dynamics, and permit optimal wind turbine designs. Some additional features of acausal modeling are:

- Building large-scale acausal models is often simplified due to the presence of drag-and-drop features available on a graphical interface. This makes the model development and reconfiguration easy and often without the need for extra derivations. In contrast, causal modeling relies on manually derived constitutive and conservation equations. This can be a tedious and potentially error-prone process in modeling large-scale multi-physics physical systems.

- A unique feature of the acausal approach is in the definition of *through* and *across* vari-

ables. A combination of such variables forms a *port*, which allows the bidirectional flow of information. Some examples of ports are, electrical, translational, etc. In the former, the current is the *through* variable and voltage is the *across* variable. In the latter, force is the *through* variable and velocity is the *across* variable. Such definitions form a conservation/constitutive law when multiple components with the same port type are connected. For instance, when multiple components with translational ports are connected at a junction, it is interpreted that the junction shares the same position and allows forces to be transmitted through it. It is notable that the *through* and *across* variables at a port model power flow through it and help implement a balance of power flow. The aforementioned bidirectionality is instrumental in facilitating acausality and admitting component-based development rather than equation-based development.

- In acausal modeling, an *a priori* knowledge of causality (what variables are known and what variables need to be computed) is not needed. This makes it easier to create and reuse models in the acausal approach. In the conventional approach, causality must be determined at the time of modeling. Example: a resistor equation, R*i = v in causal modeling, can be used in three ways i := v/R; v := R*i; R := v/i in the acausal modeling. This increases model complexity and limits the reusability of the component models.

- The acausal approach inherently provides object-oriented modeling features that are more suited to physical modeling and makes them flexible and reusable. Specifically, it facilitates model management, modularity, development of a model hierarchy, as well as parameterization. In contrast, causal approaches may require extra efforts in building such features, thereby increasing the chances of robustness and maintenance related issues.

3.2 Model Information

The wind turbine model utilized in this research is based on the IEA Wind 15-MW Reference Wind Turbine [30], a standardized reference system developed through a collaborative partnership between the National Renewable Energy Laboratory (NREL) and the Technical University of Denmark (DTU) as part of the International Energy Agency (IEA) Wind Task 37 on Systems Engineering in Wind Energy. The technical report provides a comprehensive listing of the model's parameters, which can be referenced in the Table 3.1 presenting the parameter specifications.

The wind turbine model has been structured into distinct subsystems to facilitate effective management, debugging, and modularity. Each subsystem is comprehensively described within separate libraries, including components like the tower, nacelle, gearbox, hub, and blade. These libraries are organized hierarchically, with simpler components constituting the lower tiers and more intricate ones forming the upper echelons. This hierarchical arrangement enables the deployment of various turbine configurations by straightforwardly substituting one model with another (e.g., transitioning from a rigid tower to a flexible one) without necessitating the rewriting of governing equations.

During the compilation of the model, the Modelica engine integrates the governing equations and establishes causality based on the physical laws and operating conditions inherent to the model. This modular design concept is visually represented in Fig. 3.2 and underscores the adaptability and efficiency of the wind turbine model's architecture.

3.2.1 Tower

The wind turbine tower is represented as a rigid body, featuring two revolute joints located at its base, which are linked to a spring and damper system. These revolute joints enable both fore-aft and side-to-side vibrations, while the spring and damper components serve to reinforce the

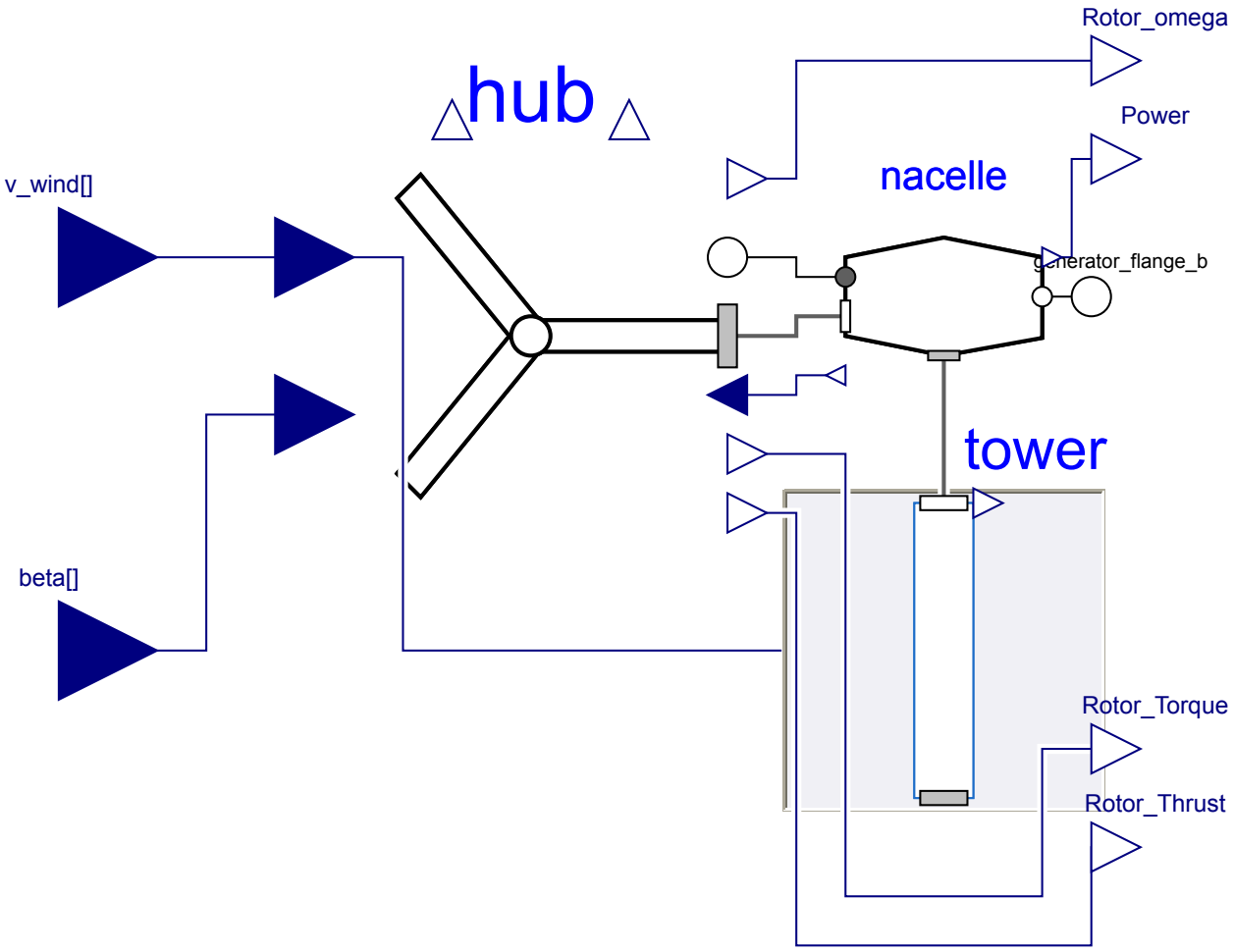

Figure 3.2: Modular wind turbine model

tower's structural integrity, aligning its natural frequency with the reference value stipulated in the IEA Wind TCP Task 37 technical report. The determination of the spring constant was achieved through the resolution of Eq.3.1.

$$k_{\text{twr}} = \omega_n^2 I_{\text{net}}, \qquad \text{where} \quad I_{\text{net}} = I_{\text{tower}} + m_{\text{tower}} r_{\text{cm,tower}}^2 + m_{\text{RNA}} L_{\text{tower}}^2. \tag{3.1}$$

Table 3.1: Turbine Parameters

Quantity	Units	Value
Rotor & Rated features		
Rotor diameter	m	242.80
Hub diameter	m	11.08
Overhang	m	10.86
Shaft tilt	$^\circ$	6
Tower to shaft	m	5.39
Rated rotor speed	rpm	7.56
Rated Rotor Torque	Nm	2e7
Wind Speed (cut in- cut out)	ms^{-1}	3.6-30
Total Rotor inertia	$kgms^2$	7.01e8
Generator inertia about high speed shaft	$kgms^2$	1.83e6
Nacelle		
Mass	kg	4.79e5
CM(CS1-x,z)	m	(4.38,4.51)
$(I_{xx}, I_{yy}, I_{zz})aboutCM$	$kgms^2$	$(1.58, 34.3, 33.3)e6$
Hub + Shaft		
Mass	kg	4.43e5
CM(CS1-x,z)	m	(-10.71,6.52)
Inertia about Shaft	$kgms^2$	7.34e6
Hub inertia about rotor axis	$kgms^2$	9.73e5

here,(CS1-x,z) represents distance from CS1 axis (shown in Fig. 3.3) in x & z direction

where k_{twr}, ω_n, and I_{net} are the tower's rotational spring constant at its base, natural frequency, and total mass moment of inertia, respectively. In addition, I_{tower}, m_{tower}, L_{tower}, $r_{cm,tower}$, and m_{RNA} are the tower's mass moment of inertia, mass, length, center-of-mass position, and the rotor-nacelle assembly mass, respectively.

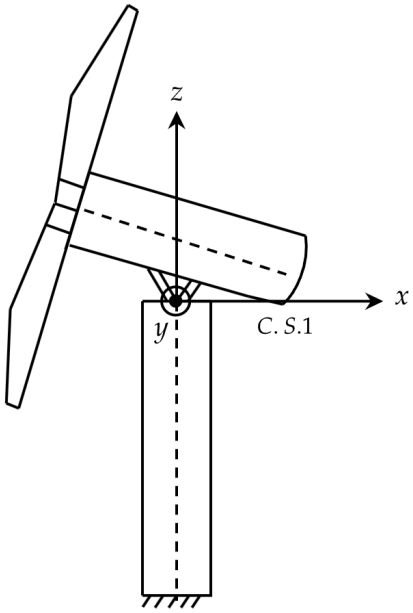

Figure 3.3: Co-ordinate system C.S.1

3.2.2 Nacelle

The nacelle is represented as a housing with inherent inertia within the model. This nacelle is affixed to the tower through a combination of a fixed-rotation element, which provides the mechanism for tilting, and a fixed-translation element, facilitating vertical displacement from the tower's apex to the rotor shaft. Within the nacelle, the gearbox is situated, modeled as a pair of rotary shafts featuring inertia attributes. These shafts are interconnected via an ideal-gear component. Notably, it's worth mentioning that the fixed-rotation, fixed-translation, revolute, and ideal-gear elements employed in this model are all part of the kinematic elements available in the Mechanics module of the Modelica Standard Library [31].

3.2.3 Hub

The hub component has been modeled as an inertia element, firmly connected to a revolute joint serving as a rotary shaft. Subsequently, the blades are affixed to the hub with an angular separation of 120 degrees between them. These blades are represented as rigid beams, discretized into multiple elements. It's important to note that this discretization primarily aims to provide a precise estimation of aerodynamic forces and moments and does not account for simulating blade flexibility.

The initial attachment of the blade involves a revolute joint that acts as the pitching mechanism. Furthermore, a position sensor is incorporated onto the blade, which continually records the blade tip's position in the inertial reference frame. This data is subsequently utilized to calculate the blade's orientation, expressed in terms of azimuth angle and any out-of-plane angular displacement due to vibrations. It's worth mentioning that the model restricts out-of-plane vibration, as it falls beyond the scope of interest for the validation purposes outlined in this thesis. Detailed design parameter values can be found in Table 3.1.

3.3 Aerodynamic Modeling

3.3.1 Orientation Angle Calculation

In order to calculate the orientation angles CRAFTS converts the blade tip position coordinates from the inertial frame to the body-fixed frame of the wind turbine blades. The inertial frame $[\mathscr{N}]$ can be transformed into the body frame $[\mathscr{B}]$ defined through the orthonormal right-hand set vector $\left[\hat{b}_1,\, \hat{b}_2,\, \hat{b}_3\right]^T$ using the rotation sequence in Eq.3.2 which is shown in Fig.3.4

$$[\mathscr{B}] = \left[R_{\psi}\right]\left[R_{\beta}\right][R_{\Phi}][R_{\Lambda}][R_{\Gamma}][R_{\Psi}][\mathscr{N}] \tag{3.2}$$

$$[R_{\Gamma}] = \begin{bmatrix} \cos(\Gamma) & 0 & -\sin(\Gamma) \\ 0 & 1 & 0 \\ \sin(\Gamma) & 0 & \cos(\Gamma) \end{bmatrix}; [R_{\Lambda}] = \begin{bmatrix} 1 & 0 & 0 \\ 0 & \cos(\Lambda) & \sin(\Lambda) \\ 0 & -\sin(\Lambda) & \cos(\Lambda) \end{bmatrix} \tag{3.3a-b}$$

$$\left[R_{\beta}\right] = \begin{bmatrix} \cos(\beta) & -\sin(\beta) & 0 \\ \sin(\beta) & \cos(\beta) & 0 \\ 0 & 0 & 1 \end{bmatrix}; \left[R_{\psi}\right] = \begin{bmatrix} \cos(\psi) & 0 & -\sin(\psi) \\ 0 & 1 & 0 \\ \sin(\psi) & 0 & \cos(\psi) \end{bmatrix} \tag{3.4a-b}$$

where the angles Ψ, Γ, Λ, Φ, β, and ψ represent the yaw, tilt, azimuth, blade precone, airfoil pitch, and flap-wise deflection angles, respectively. The rotation matrices described in Eq. (3.3 and 3.4) are used to perform the transformation. In this work, $[R_{\Psi}] = [\, I \,]$ due to the assumed no yaw-misalignment condition, and $[R_{\Phi}] = [\, I \,]$ due to the assumed no precone. Detailed discussions regarding the co-ordinate system transformation can be found in [32].

$$\sin(\psi) = \frac{r_x \cos(\Gamma) - r_z \sin(\Gamma)}{r \cos(\beta)} \tag{3.5a}$$

$$\cos(\Lambda) = \frac{[r_z \cos(\Gamma) + r_x \sin(\Gamma)] \cos(\psi) - r_y \sin(\psi) \sin(\beta)}{r \left[\cos^2(\psi) + \sin^2(\psi) \sin^2(\beta)\right]} \tag{3.5b}$$

$$\sin(\Lambda) = -\frac{[r_z \cos(\Gamma) + r_x \sin(\Gamma)] \sin(\psi) \sin(\beta) + r_y \cos(\psi)}{r \left[\cos^2(\psi) + \sin^2(\psi) \sin^2(\beta)\right]} \tag{3.5c}$$

$$\begin{aligned} \tan(\Lambda) &= \frac{\sin(\Lambda)}{\cos(\Lambda)} \\ &= -\frac{[r_z \cos(\Gamma) + r_x \sin(\Gamma)] \sin(\psi) \sin(\beta) + r_y \cos(\psi)}{[r_z \cos(\Gamma) + r_x \sin(\Gamma)] \cos(\psi) - r_y \sin(\psi) \sin(\beta)} \end{aligned} \tag{3.5d}$$

With the tilt angle Γ and blade pitch angle β given, the model calculates the azimuth Λ and flap-wise deflection ψ using the blade-tip position in the inertial frame, $[P]^{\mathcal{N}} = [r_x,\ r_y,\ r_z]^T$. This calculation was done to prevent inconsistent values obtained using the corresponding angle sensors, and is shown in Eq. 3.2.

Given the tilt and pitch angles Γ and β, respectively, solve Eq.3.5a for ψ, which in turn allows evaluating Eq.3.5d for Λ, giving rise to expressions for the flap-wise and azimuth angles. Modelica libraries are able to perform all of these transformations automatically, but in order to enhance readers' comprehension of he model development process, we have included some analytical formulas in this study.

With the orientation angles determined, the forces and moments acting on the blades can be evaluated. Each blade is then discretized into a number of elements. In this work, we choose 28 elements.

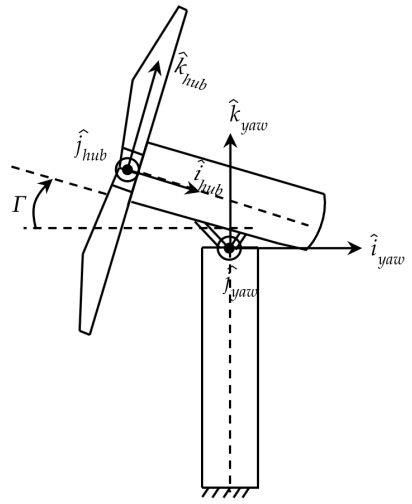

(a) Tilt aligned co-ordinate system

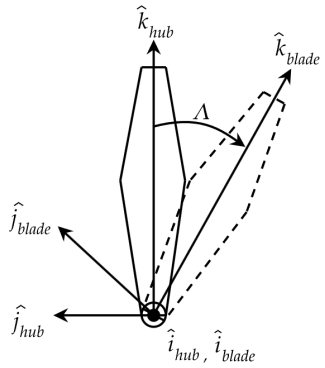

(b) Azimuth aligned co-ordinate system

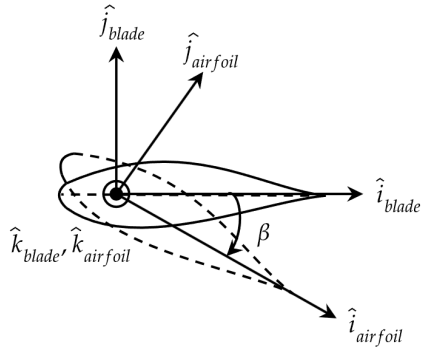

(c) Pitch aligned co-ordinate system

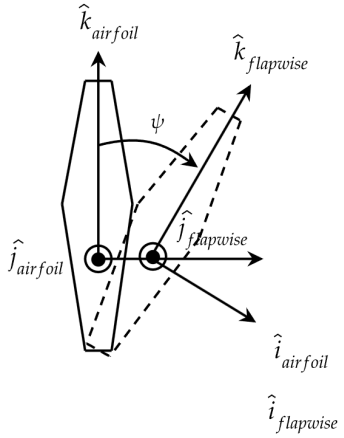

(d) Flap-wise aligned co-ordinate system

Figure 3.4: Co-ordinate system transformation from inertial frame to body-fixed frame

3.3.2 Finding Force and Moments in the Rotational plane

Within the blade element, a rotation matrix is constructed that transforms the wind velocity and the blade element's linear velocity from the inertial frame, $[\mathscr{N}]$, defined through the orthonormal right-hand set vector $\left[\hat{i},\ \hat{j},\ \hat{k}\right]^T$ to the intermediate plane of rotation, $[\mathscr{I}]$, defined through the

orthonormal right-hand set vector $\left[\hat{i}',\ \hat{j}',\ \hat{k}'\right]^T$ for each blade element (In our case azimuth aligned co-ordinate system is the plane of rotation frame). With those two values available, the relative wind velocity of the wind with respect to the blade element in the plane of rotation is computed by Eq.3.6c

$$\left[V_{w/b}\right]^{\mathscr{N}} = [V_w]^{\mathscr{N}} - [V_b]^{\mathscr{N}} \tag{3.6a}$$

$$\left[V_{w/b}\right]^{\mathscr{I}} = [R_\Lambda]\,[R_\Gamma]\,[R_\Psi]\left[V_{w/b}\right]^{\mathscr{N}} \tag{3.6b}$$

$$\|V^{\mathscr{I}}_{w/b}\| = \sqrt{V_x^2\,(1-a)^2 + V_y^2\,(1+a')^2} \tag{3.6c}$$

where $\left[V_{w/b}\right]^{\mathscr{N}}$ is the velocity of wind relative to the blade in the inertial frame, $[V_w]^{\mathscr{N}}$ and $[V_b]^{\mathscr{N}}$ are the velocities of wind and blade, respectively, in the inertial frame, $\left[V_{w/b}\right]^{\mathscr{I}}$ is the velocity of the wind with respect to the blade in the intermediate plane of rotation, and lastly $[R_\Lambda]\,[R_\Gamma]\,[R_\Psi]$ is the rotation matrix that transforms inertial frame to the intermediate plane of rotation.

An iterative procedure is then called to compute the axial and tangential induction factors at each blade element. Once the procedure converges, V_x and V_y, which are the projections of $\left[V_{w/b}\right]^{\mathscr{I}}$ into the intermediate plane of rotation, are updated to take into account the induced velocity as in 3.6c. This iterative approach is based on the work done by Ning et al. [33], which is also the approach implemented in AeroDyn by NREL [34]. The forces and moments generated by each blade element at the intermediate plane of rotation can be computed as in Eq.3.7,

$$\begin{aligned} F_x^{\mathscr{I}} &= \ \ {}^1\!/_2\rho A_{blade} C_N \left\|V^{\mathscr{I}}_{w/b}\right\|^2; \quad M_x^{\mathscr{I}} = -rF_y^{\mathscr{I}} \\ F_y^{\mathscr{I}} &= -{}^1\!/_2\rho A_{blade} C_T \left\|V^{\mathscr{I}}_{w/b}\right\|^2; \quad M_y^{\mathscr{I}} = \ \ rF_x^{\mathscr{I}} \end{aligned} \tag{3.7}$$

where $F^{\mathscr{I}}$ and $M^{\mathscr{I}}$ are the forces and moments in the intermediate plane of rotation, respectively, and r is the radial distance from the blade root to the blade element.

3.3.3 Local Force and Moment Calculation

After the evaluation of $F^{\mathscr{I}}$ and $M^{\mathscr{I}}$ in the intermediate plane-of-rotation, as given in Eq.3.7 ,a rotation sequence is subsequently used to align the forces in the body-fixed frame of the blade segment by considering the pitch, local twist, and flap-wise deflection angles.

$$[F]^{\mathscr{B}} = \left[R_{\psi}\right]\left[R_{\beta+\theta}\right][F]^{\mathscr{I}} \tag{3.8a}$$

$$[M]^{\mathscr{B}} = \left[R_{\psi}\right]\left[R_{\beta+\theta}\right][M]^{\mathscr{I}} \tag{3.8b}$$

where θ in Eq.3.8a and Eq.3.8b represents the local twist at a blade element. With the forces and moments properly resolved in the appropriate frame, all the generated forces and moments from the output of the discretized blade elements are added. The sum of those forces and moments is then applied on the blade, generating the thrust and torque, inducing the rotation of the low speed rotary shaft, generating electricity on the high-speed shaft end.

CHAPTER 4: CONTROL MODULE

A control module has been developed in CRAFTS to facilitate performance analysis and control co-design for wind turbines. This user-friendly, computationally-efficient module allows various control algorithms (e.g., ROSCO controller, CRAFTS nonlinear controller) to be implemented and/or interact with the turbine dynamics.

4.1 ROSCO Controller

ROSCO is an open-source reference controller with industry-standard functionality for wind turbine control that is developed and maintained by NREL [20]. In ROSCO, the control laws are divided into two regimes: below-rated (regime 2) and above-rated (regime 3) wind speeds. In regime 2, ROSCO employs a generator torque actuation using a feedback PI controller that regulates the rotor speed around the optimum tip-speed ratio as in Eq.4.1,

$$\omega_{ref}(V) = GR\frac{\lambda_{opt}V}{R} \tag{4.1}$$

where, GR is the gearbox ratio, λ_{opt} is the optimum tip-speed ratio corresponding to maximum power coefficient $C_{p,opt}$, R is the rotor radius, and V is the wind velocity, which is directly taken from the wind model. Thus, when the rotor angular velocity tracks this reference angular velocity, energy extraction is maximized. This leads to the following generator torque relationship described in Eq.4.2.

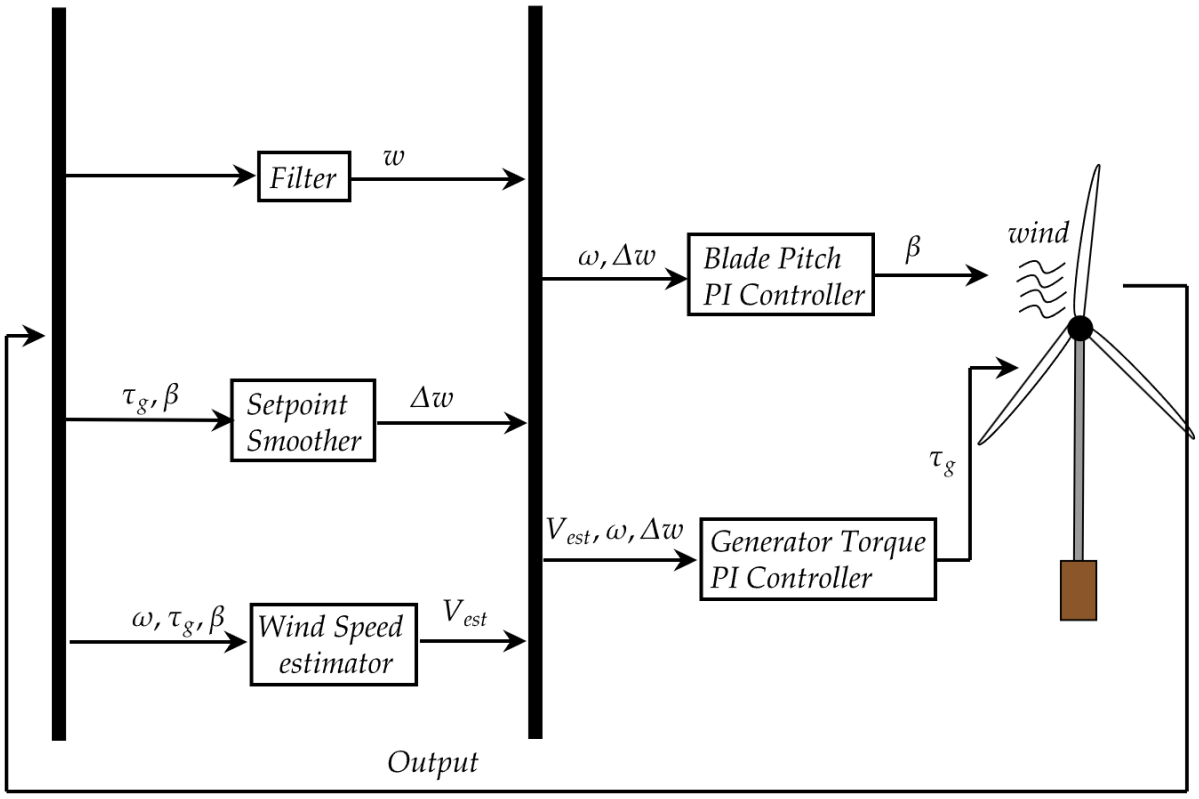

Figure 4.1: Schematic diagram of ROSCO Controller

$$\tau_g(t) = K_{P,vs} e(t) + K_{I,vs} \int e(t)\, dt \ , \quad \text{where } \ e(t) = \omega_{ref}(V) - \omega \tag{4.2}$$

In regime 3, ROSCO uses a collective blade pitch actuation to maintain the power output at the rated value. This is achieved via a gain-scheduled feedback PI controller as shown in Eq.4.3,

$$\beta(t) = K_{P,pc} e(t) + K_{I,pc} \int e(t)\, dt \ , \quad \text{where } \ e(t) = \omega_{rated} - \omega \tag{4.3}$$

Furthermore, ROSCO utilizes a set point smoother to allow for a smooth transition between the two regimes of operation by shifting the rotor speed set point of the saturated controller when the unsaturated controller is active. Perturbation in rotor speed set point is defined by the following equation:

$$\Delta w = (\beta - \beta_{min}) K_{vs} - (\tau_{g,rat} - \tau_g) K_{pc} \tag{4.4}$$

Shifting of the set point is regulated by the two parameters k_{vs} and k_{pc}.In below-rated operation, $\Delta\beta = 0$ and in above rated operation, $\Delta\tau = 0$. Then a piece-wise logic is applied to shift the controller set point as following manner as Eq.4.5.

$$\omega_{ref,\tau} = \begin{cases} \omega_{ref,\tau} - \Delta\omega & \Delta w \geq 0 \\ \omega_{ref,\tau} & \Delta w < 0 \end{cases} \text{ and, } \omega_{ref,\beta} = \begin{cases} \omega_{ref,\beta} & \Delta w \geq 0 \\ \omega_{ref,\tau} - \Delta w & \Delta w < 0 \end{cases} \tag{4.5}$$

For the PI gain scheduling of the collective pitch controller, ROSCO uses numerical linearization of the generator speed dynamics and the tuning algorithm used in ROSCO is available as an open-source code in the OpenFAST GitHub [22] repository. The interaction between ROSCO and CRAFTS is achievable using the Functional Mock-up Interface Unit, a free standard that defines a container and an interface to exchange dynamic models [35].

From the open-source code mentioned above we can find the gain scheduled PI controller gains in torque and pitch control using the ROSCO tuning procedure (Fig. 4.2).

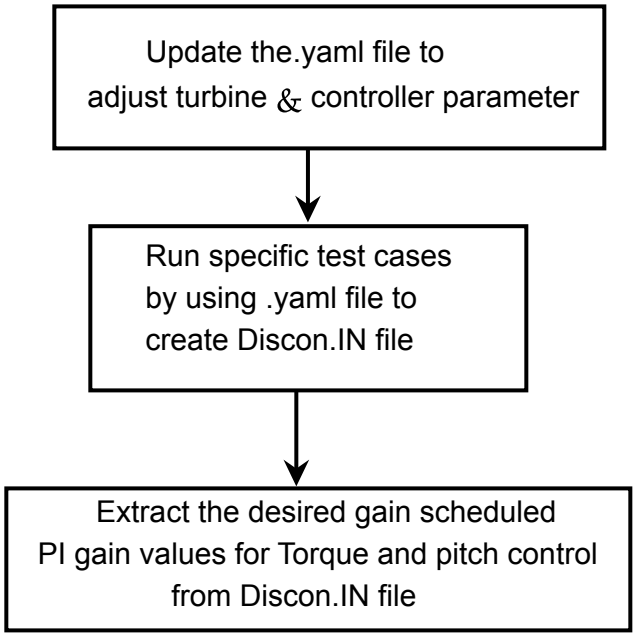

Figure 4.2: ROSCO tuning procedure

4.2 Nonlinear Controller

The section describes a built-in nonlinear controller that was developed in CRAFTS for multi-regime operations of variable-speed wind turbines. One of the main elements of novelty is that the controller utilizes four tunable parameters and does not require gain scheduling, which is a common technique used in control design. The controller was developed using Lyapunov stability analysis of the resulting equilibria, and the regions of attraction of the equilibria were determined, which allows stable switching between operating regimes (2, 2.5, and 3), as shown in our previous work [36]. This is a significant improvement to ensure stable switching between regimes. Another element of novelty is that the controller does not require the sensed wind velocity, which simplifies the control system and reduces the cost of the turbine. Overall, the development and evaluation of this nonlinear controller provide a significant contribution to the field of wind turbine control design.

In regime 2, the CRAFTS nonlinear controller maximizes power production by tracking the optimum tip-speed ratio λ_{opt}. Here the generator torque control input T_g is given by Eq. (4.6a)

$$Regime-2\ Torque: T_g GR = k_t \omega_r^2\ , \quad \text{where}\ \ k_t = k_{t,opt} = \frac{1}{2}\rho A_{rotor} R^3 \frac{C_{p,opt}}{\lambda_{opt}^3} > 0 \qquad \text{(4.6a-b)}$$

where GR and ω_r are the gearbox ratio and measured rotor angular velocity, respectively. From Eq. (4.6b), prior knowledge of all the parameters required to compute the control gain k_t is available. For instance, the air density ρ, the rotor swept area A_{rotor}, and the rotor radius R are all known. Furthermore, the optimal power coefficient and tip-speed ratios, $C_{p,opt}$ and λ_{opt} respectively, are obtained using the C_P — λ curves shown in Fig.5.5a and Fig.5.5b. However, the value for k_t is not exact at all times and may change over time due to blade erosion and residue buildup, nonetheless the value obtained through Eq. (4.6b) provides a good approximation of the gain value.

In addition to the generator torque actuation, the blade pitch modulation in 4.7 is proposed to allow the controller to transition from regime 3 back into regime 2 by bringing the current blade pitch β to the lower limit of β_0. This pitch modulation occurs only during the transition period to maintain the pitch angle at its lower limit. To transition from regime 2 to regime 3 control, and vice versa, a switching point based on the rotor speed is proposed in Eq.4.8.

$$Regime-2\ Pitch:\ \dot{\beta} = -k_{p,2}\left(\beta - \beta_0\right), \quad k_{p,2} > 0 \tag{4.7}$$

$$Switching\ Speed:\ \omega_{r,sw} = \left(\frac{P_{ref}}{k_t}\right)^{1/3} \tag{4.8}$$

when the rotor angular velocity ω_r becomes greater than the switching angular velocity $\omega_{r,sw}$, the control law switches from regime 2 to regime 3 control. Alternatively, when the rotor angular velocity ω_r becomes less than the switching angular velocity $\omega_{r,sw}$, the control law switches from regime 3 to regime 2 control. Based on this observation, we define a switching condition whose output acts as a switching command between regime 2 & 3 defined by Eq.4.9.

$$\begin{aligned} &if\ w_r - w_{r,sw} \geq 0;\ then\ Sw_{out} = 1; \\ &else\ Sw_{out} = 0; \end{aligned} \tag{4.9}$$

In regime 3, the generator torque and collective pitch control are both modulated such that the turbine output is tracking the rated (reference) power P_{ref}. This is achieved by applying the control torque such that the generator is operating at its rated torque value as described in Eq.4.10.

$$Regime-3\ Torque:\ T_g = \frac{P_{ref}}{\omega_r\ GR} \tag{4.10}$$

In addition, a collective blade pitch modulation in Eq.4.11 is performed to maintain the rotor at its

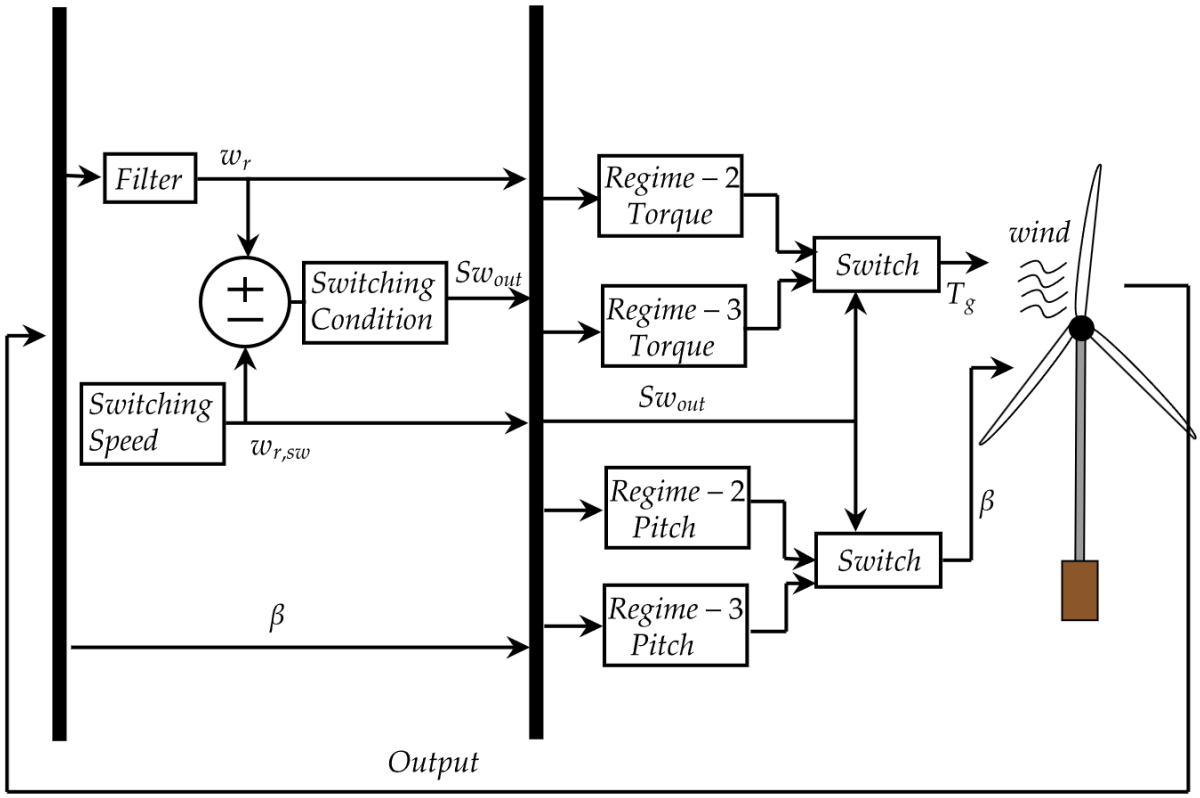

Figure 4.3: Schematic diagram of Non-linear Controller

rated speed.

$$Regime-3\ Pitch:\ \beta = \beta_0 + k_{p,3}\left(\omega_r^2 - \omega_{r,sw}^2\right) + k_{i,3}\int_{t_0}^{t}\left(\omega_r^2 - \omega_{r,sw}^2\right)dt \tag{4.11a}$$

$$\dot{\beta} = 0 \text{ if } \begin{cases} \beta \leq \beta_0 & \text{and} \quad \omega_r < \omega_{r,sw} \\ \beta \geq \beta_{max} & \text{and} \quad \omega_r > \omega_{r,sw} \end{cases} \tag{4.11b}$$

where $k_{p,3},\ k_{i,3} > 0$ are constants, β_{max} denotes an upper limit of β, β_0 is the lower limit of pitch angle. In Eq.4.11, the squared error between the current rotor speed and the switching speed is taken into consideration. The error is then modulated by PI controller gains, allowing the model to reach the reference speed. These positive PI gains are determined via a simple trial-and-error and a gain scheduling is not used. Through Lyapunov stability analysis, the stability of the equilibria in the presence of the two independently functioning torque- and pitch-control feedback loops was proven in our previous work [36]. Overall control structure of non-linear controller is represented through a schematic diagram in Fig.4.3.

CHAPTER 5: MODEL VALIDATION

The validation process of the CRAFTS model encompassed a series of test cases consisting of both open-loop and closed-loop testing scenarios designed to rigorously assess its performance in comparison to the extensively validated industry-standard platform, OpenFAST [22]. This validation initiative was a part of the FOCAL Campaign 1 [23], which is primarily dedicated to the validation of land-based wind turbine systems. Though this thesis only shows the comparison of CRAFTS performance with that of OpenFAST [22], the simulation outcomes produced by the CRAFTS simulator under these test cases have been compared with the results of other participants of campaign 1 as well as demonstrated in [24]. These findings were pivotal for evaluating the accuracy of the wind turbine in aerodynamic, structural as well as in control aspects, resulting in the identification of multiple areas for enhancement in the CRAFTS model. The subsequent implementation of these improvements through model modifications have significantly enhanced the overall performance of CRAFTS.

Test scenarios for assessing the performance of the CRAFTS model have been developed through collaborative efforts involving multiple research entities participating in a project supported by the United States Department of Energy's Advanced Research Projects Agency for Energy (ARPAE). Specifically, the test cases were structured as follows:

- Test Case (TC) 1.x was crafted to scrutinize the response of the wind turbine in relation to variations in rotor speed.
- Test Case (TC) 2.x was structured to investigate how the wind turbine responds to varying pitching maneuvers.
- Test Case (TC) 3.x was devised to ensure the compatibility of CRAFTS model with control

Table 5.1: Test Cases

Test Case	Scenario	Wind Speed (m/s)	Pitch (degrees)	Rotor Control (rpm)
TC 1.x	1	12.83	0	Ramp 3 to 10
	2	12.83	10	Ramp 3 to 10
	3	18.39	9	Ramp 3 to 10
	4	18.39	15	Ramp 3 to 10
TC 2.x	1	27.69	step -2 to 30	Locked
	2	12.83	step ± 2 from 0	7.56
	3	18.41	step 10 to 14	7.56
	4	12.83	Ramp -1 to 5	7.56
	5	18.41	Ramp 10 to 16	7.56
TC 3.x	1	Step 8-30-8	-	Rosco Controller
	2	TR1 Gust	-	Rosco Controller
	3	TR1 Steady 12.83	-	ROSCO Controller
	4	TR1 Sinusoidal	-	ROSCO Controller
	5	TR1 Spectral	-	ROSCO Controller
	6	TR1 Spectral	-	ROSCO Controller

system design and to evaluate the performance of the turbine control system using ROSCO under distinct wind conditions.

TC 1.x and TC 2.x are designed to evaluate the open-loop performance of CRAFTS model that served as a integral components in the verification process, validating the intrinsic characteristics of the turbine model and ensuring consistent aerodynamic performance. In contrast, TC 3.x was specifically tailored to assess the turbine model's behavior under closed-loop scenarios, where active control mechanisms were integrated ensuring its ability to control system design and performance validation under closed-loop scenarios. For a comprehensive elucidation of each test case, we direct readers to the comprehensive details provided in Table 5.1.

5.1 TC 1.x Validation

Within Test Case 1.x, the CRAFTS model underwent evaluation in an open-loop configuration, during which the rotor speed exhibited a range of variation from 3 RPM to 10 RPM, while maintaining consistent wind speed and pitch angle values. The outcomes obtained through the validation process in TC 1.x not only serve the purpose of appraising the performance of the CRAFTS model but also hold significance in delineating specific turbine attributes crucial for the design of control systems. The validation results for TC 1.x, in comparison to the data generated by OpenFAST, are depicted in Fig.5.1-5.4. Notably, the CRAFTS model's performance closely aligns with that of OpenFAST. Specifically, there is a strong agreement in aerodynamic thrust and torque values across all load cases, with minor disparities occurring at higher RPM values for aerodynamic torque. Additionally, the forces and moments exhibit analogous trends with substantial overlap compared to the data reported by OpenFAST in Fig. 5.1 through 5.4. However, discernible deviations emerge in the tower top moments, primarily along the z-axis and marginally along the x and y axes at higher rotational speeds, as shown in Fig. 5.1. In Fig. 5.2, the observed deviation demonstrates a decreasing trend with increasing pitch angle. Additionally, Fig. 5.3 and 5.4 present a similar scenario, where it becomes evident that for higher wind speeds, the deviations between CRAFTS and OpenFAST tower top forces and moments are less pronounced than in lower wind conditions

Furthermore, we can establish certain fundamental characteristics of the turbine, as outlined in Table 3.1 from TC 1.x. For instance, when the wind turbine operates at its rated rotor speed, we anticipate the turbine to manifest the rated torque and rated thrust as specified. So from Fig.5.1, we can observe that the aerodynamic torque of the CRAFTS model reaches its peak value at the rated rotor speed of 7.56 RPM. Similarly, the aerodynamic thrust achieves a peak value within the range of 2.75 MN to 2.80 MN, which closely matches the figures reported for the IEA 15MW turbine.

Future investigations will focus on resolving the minor discrepancies between CRAFTS and OpenFAST in case aerodynamic torque and tower top force and moments. One avenue to explore involves the integration of a more intricate aerodynamics model within CRAFTS, capable of accounting for factors beyond induction losses. Here, we have previous implemented static blade element theory which we are planning to update with dynamic blade element theory. This enhancement is expected to further refine the model's predictive capabilities. Nonetheless, it's essential to acknowledge that CRAFTS currently provides an accurate representation of the trends observed in OpenFAST, making it well-suited for control co-design exercises in its present form.

Additional crucial performance metrics for wind turbine design include the power coefficient, denoted as C_P, and the thrust coefficient, marked as C_T as defined by Eq.5.1 which provide essential information for control system design and helps to explore different aerodynamic behavior of the turbine.

$$C_P = \frac{Actual\ Power\ produced\ by\ turbine}{Power\ Available\ in\ the\ turbine} = \frac{P}{1/2\ \rho A v^3} \tag{5.1a}$$

$$C_T = \frac{Thrust\ Force}{Dynamic\ Force} = \frac{T}{1/2\ \rho A v^2} \tag{5.1b}$$

Here, $\rho, A,$ *and* v corresponds to air density, area of the rotor and wind speed respectively. These coefficients are analyzed in relation to the tip speed ratio, $\lambda = \frac{wr}{v}$, or TSR by systematically adjusting the pitch angle. For each specific pitch angle wind turbine is operated for range of rotor speed and the corresponding power and thrust generated is determined which by using Eq.5.1 would provide a $C_P vs \lambda$ & $C_T vs \lambda$ curve for each specific pitch angle. Using this procedure results encompassing the power and thrust coefficients were generated and subsequently compared to the data obtained from OpenFAST.

The outcomes of this comparative analysis are illustrated in Fig.5.5a-5.6b, revealing a notably

strong agreement between the results produced by CRAFTS and those from OpenFAST. However, we can notice some deviation in results at higher tip speed ratio that occurs for higher rotational speed. These deviations can be attributed to the similar reasoning that occurs in TC 1x. We anticipate that introducing dynamic blade element momentum theory would result in a reduction of this deviation . Moreover, the results obtained from the $C_P - C_T - \lambda$ curve can provide valuable insights into the torque and thrust characteristics exhibited by the CRAFTS model in the TC 1.x simulation scenario.

Let's discuss the relationship between the aerodynamic torque versus rotor speed graph, as demonstrated in Fig.5.1, in the context of the C_P versus λ characteristics. In a scenario with a constant wind speed and pitch angle, an increase in rotor speed leads to a continuous rise in the value of λ. Consequently, the power coefficient, denoted as C_p, follows a pattern akin to the C_P versus λ curve, illustrated in Fig. 5.5a for a pitch angle of 0°. This results in an increase in power output until reaching the optimal λ (the point at which C_P is maximized), followed by a decrease.

As rotor speed steadily increases, the sole means to curtail power production is by reducing the aerodynamic torque. Therefore, in the aerodynamic torque versus rotor speed graph demonstrated in Fig.5.1, one would anticipate an initial increase in aerodynamic torque, followed by a decrease after reaching a certain peak value corresponding to the rotor speed that aligns with the optimal λ. From Fig.5.5a, we can notice that the optimal λ value is approximately 7.49, which corresponds to a rotor speed of 7.56 *rpm*. This observation explains the increasing trend in aerodynamic torque in Fig.5.1 up to 7.56 *rpm*, followed by a declining trend. Similarly we can comprehend the trend of aerodynamic thrust versus rotor speed of Fig.5.1 in the context of Fig. 5.6a.

Finally, the derivatives, which represent the sensitivities of rotor thrust and generator torque with respect to rotor speed, play a crucial role in determining the control gains used in various controller algorithms such as ROSCO controller uses these sensitivity characteristics in determining the pro-

portional and integral gains. These sensitivities have been computed and are showcased in Fig.5.7 revealing a strong alignment with the data obtained from OpenFAST.

5.2 TC 2.x Validation

Within TC 2.x, a comprehensive investigation was conducted to assess the wind turbine's response to certain open-loop conditions by varying pitching maneuvers while maintaining a constant wind speed and rotor speed. The same pitch maneuvers were executed both in OpenFAST and CRAFTS, encompassing a series of step-input and ramp-input pitch commands in various operational wind speed regions, including those below and above the rated wind speed.

As shown in Fig. 5.8-5.12, the results derived from CRAFTS exhibit a notable concordance with the findings obtained from OpenFAST. These results follow the same overarching trends and magnitudes as OpenFAST but reveal some divergence in the aerodynamic torque and minor divergence in aerodynamic thrust. This divergence can be attributed to the distinctive airfoil modeling approaches employed by CRAFTS (utilizing a linear blade/airfoil model) and OpenFAST (incorporating an unsteady blade/airfoil model). Moreover, we can interpret the patterns observed by CRAFTS and OpenFAST in the test scenarios of TC 2.x within the context of the C_P versus λ and C_T versus λ curves.When varying the pitching angle while maintaining constant rotor speed and wind speed, the parameter λ remains constant throughout the entire operating range. However, it's important to note that the coefficient of power C_P will vary with changes in the pitching angle. Specifically, from the C_P versus λ curve we can notice that increase in the pitching angle towards higher values will lead to a lower C_P at the constant λ, resulting in a decrease in torque. Conversely, decreasing the pitching angle towards lower values will cause an increase in C_P, leading to an increase in aerodynamic torque. So, we can observe that for a constant λ, aerodynamic torque is inversely proportional to the pitching angle. From TC 2.5 of Fig.5.12, we can observe that when the pitching angle increases aerodynamic torque decreases and vice versa. Similar incident occurs for other cases of TC 2.x as well except 2.1 shown in Fig. 5.8 as in this case rotor speed is locked so it doesn't follow the characteristics of C_P versus λ for varying pitching angle. Similar

comprehensive analysis can be done for aerodynamic thrust as well.

Intriguingly, all test cases involving pitch commands, both increasing and decreasing, demonstrate consistent responses in CRAFTS, indicative of the absence of significant hysteresis effects. Hysteresis is a well-known effect meaning that behaviour under a change in external conditions is not symmetrical over time. This absence can be attributed to CRAFTS not utilizing stall hysteresis formulations. This verification is particularly crucial in control design, specifically when employing the ROSCO controller. In this context, the verification is necessary as it helps fine-tune the integral control gain by considering the sensitivities of thrust and torque concerning pitch values. When hysteresis effects are present, these sensitivities may differ for increasing and decreasing pitch values. Additionally, the sensitivities of thrust and torque concerning pitch, as observed in TC 2.x, are showcased in Fig.5.13. Once more, these results demonstrate a favorable alignment with the data obtained from OpenFAST.

5.3 TC 3.x validation

In TC 3.x, an assessment of the ROSCO controller performance and the wind turbine's loading characteristics under a range of wind conditions was carried out using both CRAFTS and OpenFAST models. The loading characteristics obtained from CRAFTS closely match those from OpenFAST, as evidenced by the comparative plots for TC 3.x, which are available in Fig. 5.14 through 5.19.

Test case 3.x wind profile is as following: TC 3.1 (Stepped wind), TC 3.2 (Gust), TC 3.3 (Steady), TC 3.4 (Sinusoid), TC 3.5 (Spectral), TC 3.6 (Spectral w/o setpoint smoother). Note that TC 3.1 shown in Fig. 5.14 incrementally stepped the wind speed from below-rated through the transition region into far above-rated conditions whereas in TC 3.2 shown in Fig. 5.15 wind speed remains at above rated conditions for most of the time starting from below rated condition. TC 3.3. which is shown in Fig. 5.16 focuses on the steady wind condition around the transition region (12.83 ms^{-1}) with the natural freestream turbulence characteristics (rotor-averaged turbulence intensity of 4.49% . TC 3.4 -3.6 shown in Fig. 5.17 through 5.19 demonstrates the wind turbine response in the presence of wind profile varying along the transition region .Through the examination of these test cases, it becomes evident that a comprehensive range of wind profiles, spanning various regimes of wind turbine operation, has been systematically investigated.

In TC 3.1, as shown in Fig.5.14, a controlled transition in wind speed from regime 2 to regime 3 was conducted. During the initial 4000 seconds (regime 2), the pitch angle was maintained at a constant minimum value of 1.72 degrees. This allowed the generator speed and torque to increase as the wind speed rose, ensuring the rotor operated around the optimal tip speed ratio. Subsequently, after the 4000-second mark, the wind speed transitioned from below the rated value of 12.83 ms^{-1} to an above-rated value exceeding 12.83 ms^{-1}. Concurrently, the ROSCO controller switched from generator torque actuation to collective blade pitch actuation. In regime 3, the

generator speed and torque were held constant at their rated values.

TC 3.2 illustrated how the closed-loop system responded to a sudden gust, starting from a wind speed below the rated value (8 ms^{-1}) and then reaching and maintaining a magnitude above the rated value (23 ms^{-1}). The simulations conducted in both CRAFTS and OpenFAST exhibited similar characteristics in terms of rise times, overshoot, peak values, and settling times.

We employed the same test cases, TC 3.3 and TC 3.5, from FOCAL Campaign 1 [23][24] to investigate the behavior of the wind turbine within the transition region when subjected to steady wind inputs featuring distinct turbulence characteristics. In TC 3.3, natural freestream turbulence characteristics were utilized, with a rotor-averaged turbulence intensity of 4.49%. Conversely, TC 3.5 was subjected to a manufactured Kaimal turbulence spectrum, which was generated using TurbSim based on the IEA Wind 15 MW full-scale conditions and adhering to the IEC 61400-1 standard. As observed in Fig.5.16 for TC 3.3 and Fig.5.18 for TC 3.5, the wind turbine operated at a precise pitch angle, maintaining the generator speed, torque, and thrust at their rated values.

The sole distinction between TC 3.5 and TC 3.6 lies in the deactivation of the setpoint smoother within ROSCO for TC 3.6. It is evident that the presence or absence of the setpoint smoother has minimal influence on the system's performance in these specific test cases. In TC 3.4, a wind condition characterized by sinusoidal variation with a frequency of 0.036 Hz, mimicking the pitching motion of the floating system as described in Eq.5.2, was applied to the wind turbine to assess the controller's performance. The frequency-domain analysis of the resulting rotor torque, thrust, and speed is illustrated in Fig.5.20. The maxima observed at 0.036 Hz align with expectations, as this frequency corresponds to the sinusoidal wind input. Notably, both CRAFTS and OpenFAST exhibit similar maxima in rotor speed and thrust in this context.

$$V(t) = A\sin(2\pi f \cdot t + \phi), \text{ where } \begin{cases} A = 0.68\ ms^{-1} \\ f = 0.036\ Hz \end{cases} \tag{5.2}$$

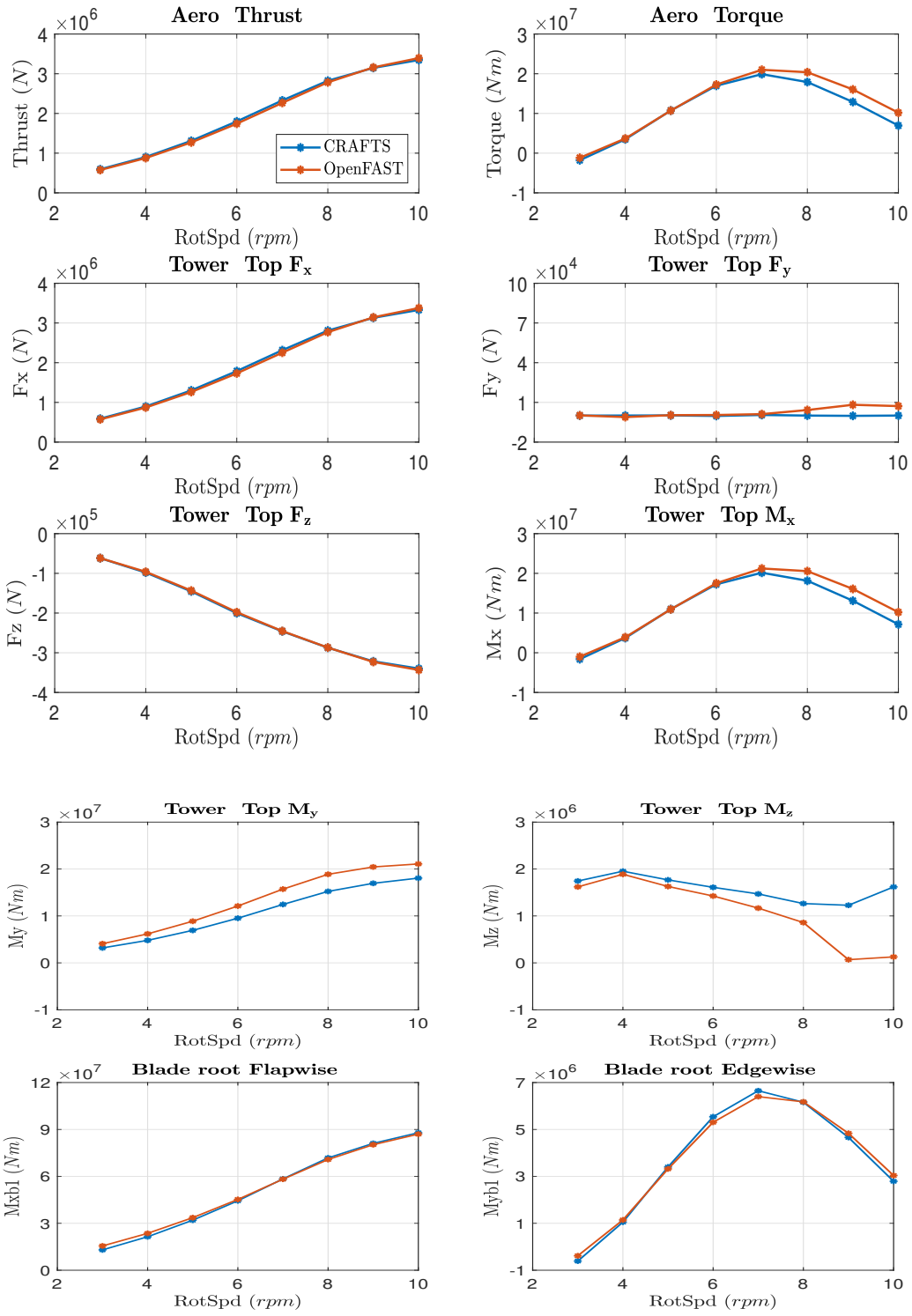

Figure 5.1: Test Case 1.1: $V_\infty = 12.83ms^{-1}, \beta = 0°$

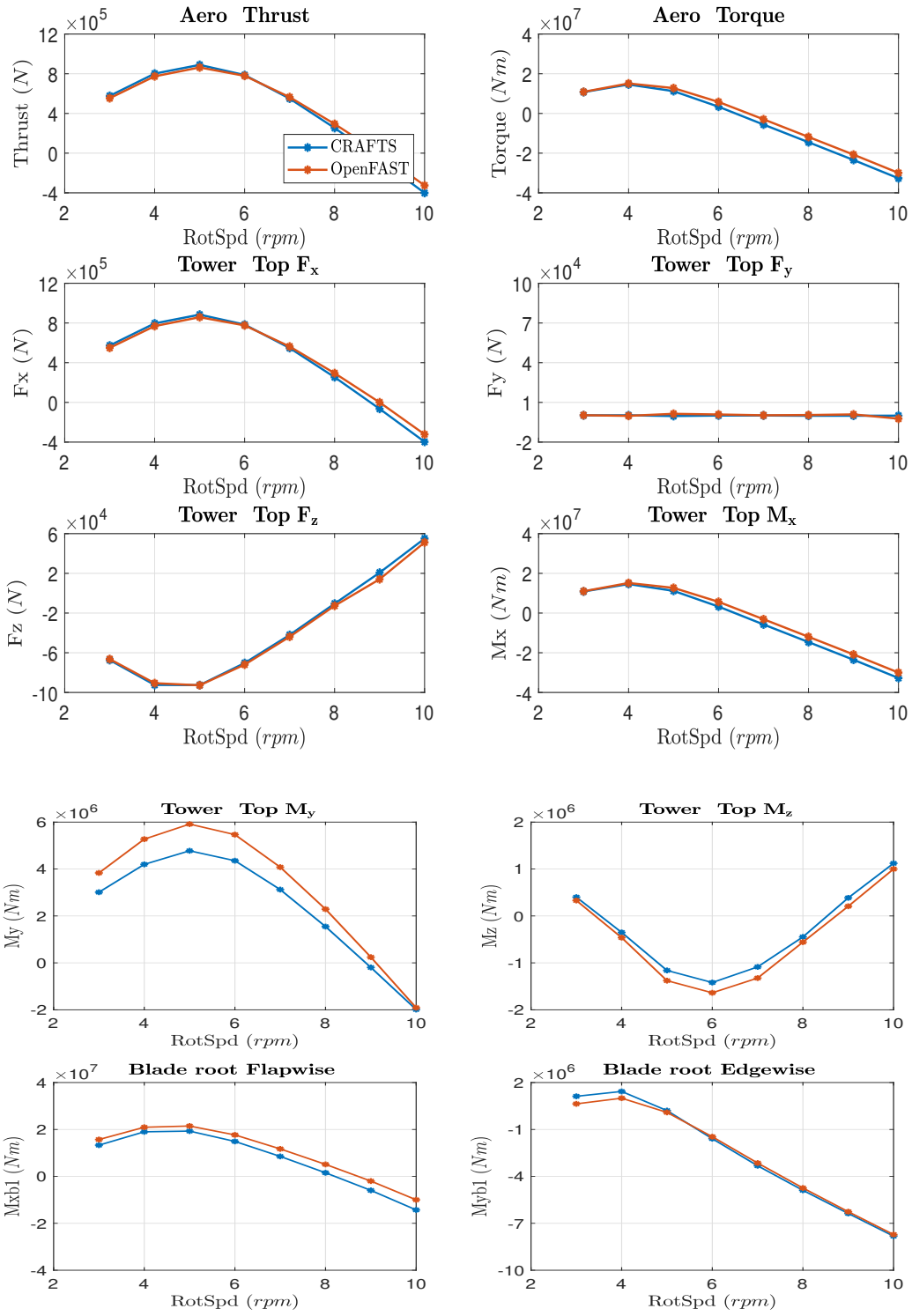

Figure 5.2: Test Case 1.2: $V_\infty = 12.83ms^{-1}, \beta = 10^\circ$

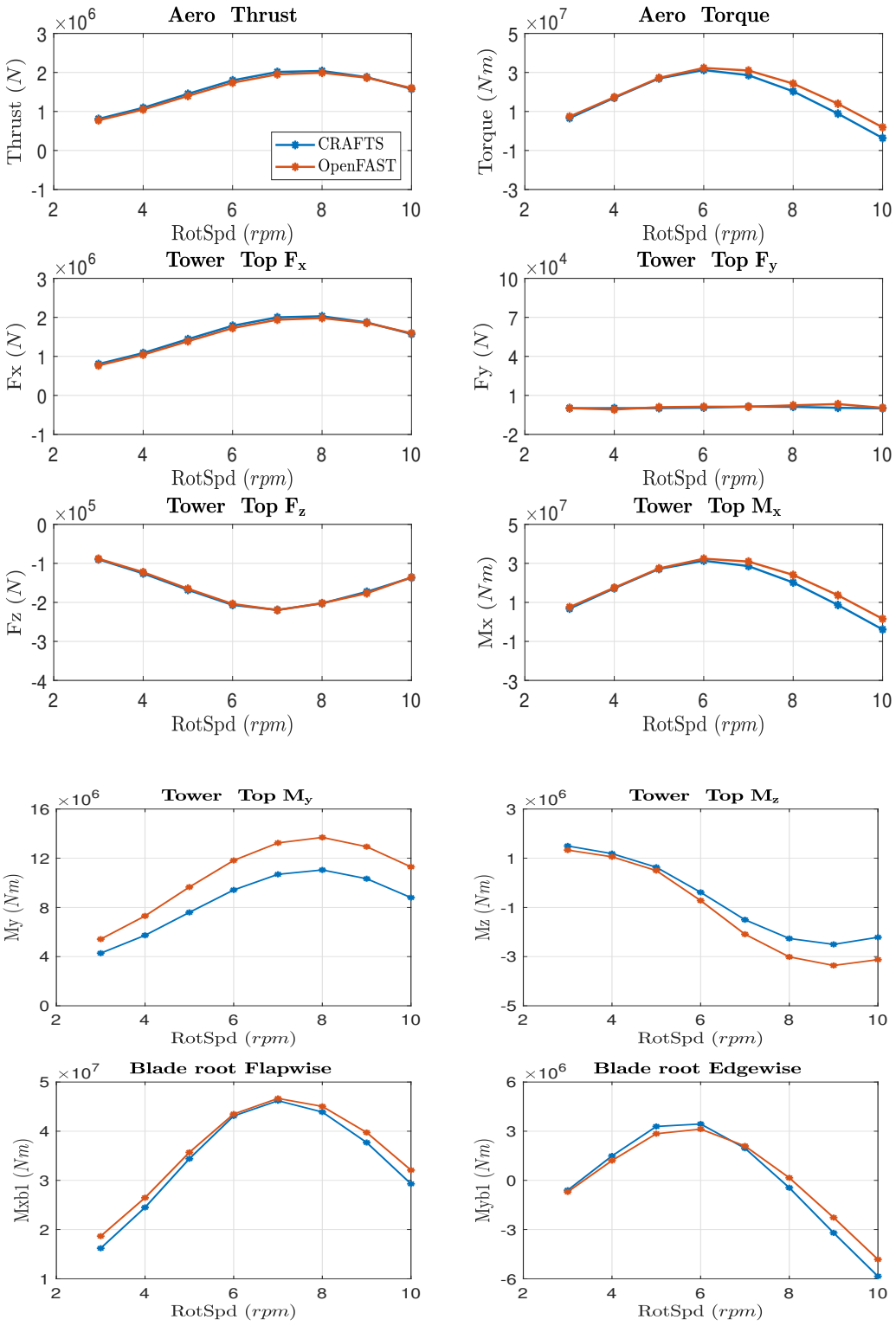

Figure 5.3: Test Case 1.3: $V_\infty = 18.39ms^{-1}, \beta = 9^\circ$

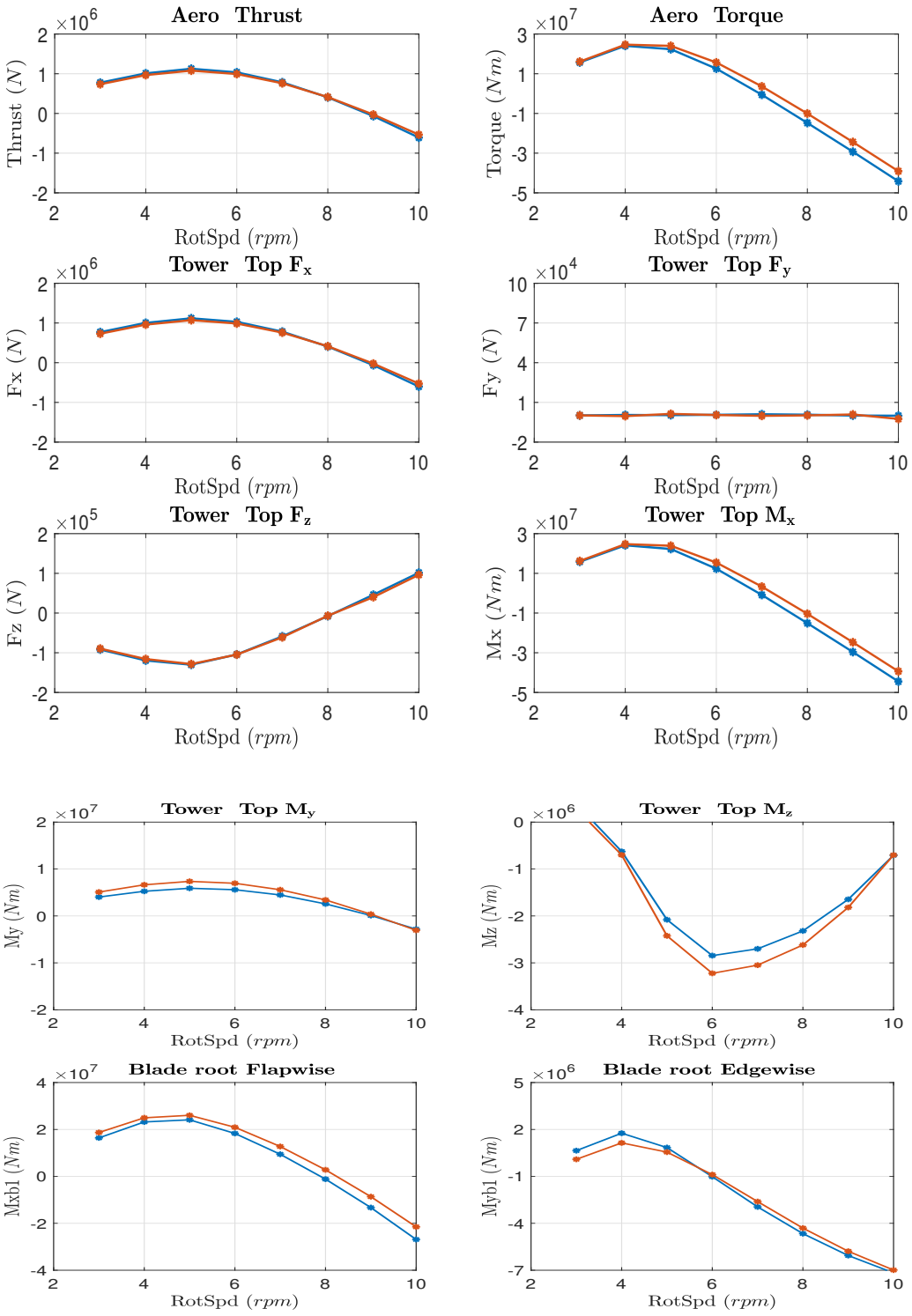

Figure 5.4: Test Case 1.4: $V_\infty = 18.39ms^{-1}, \beta = 15°$

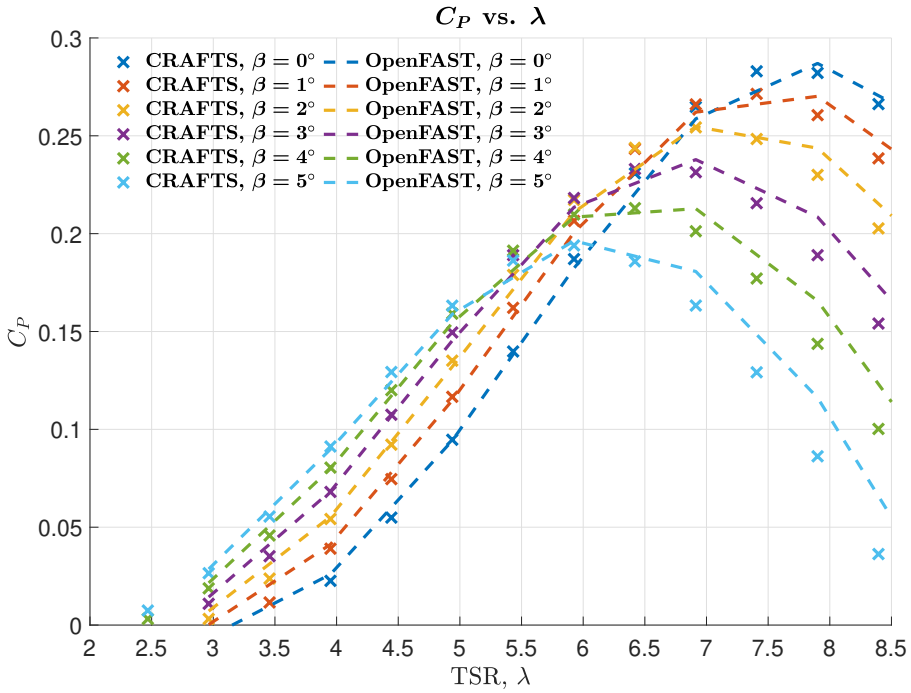

(a) C_P Vs λ for low pitch angles

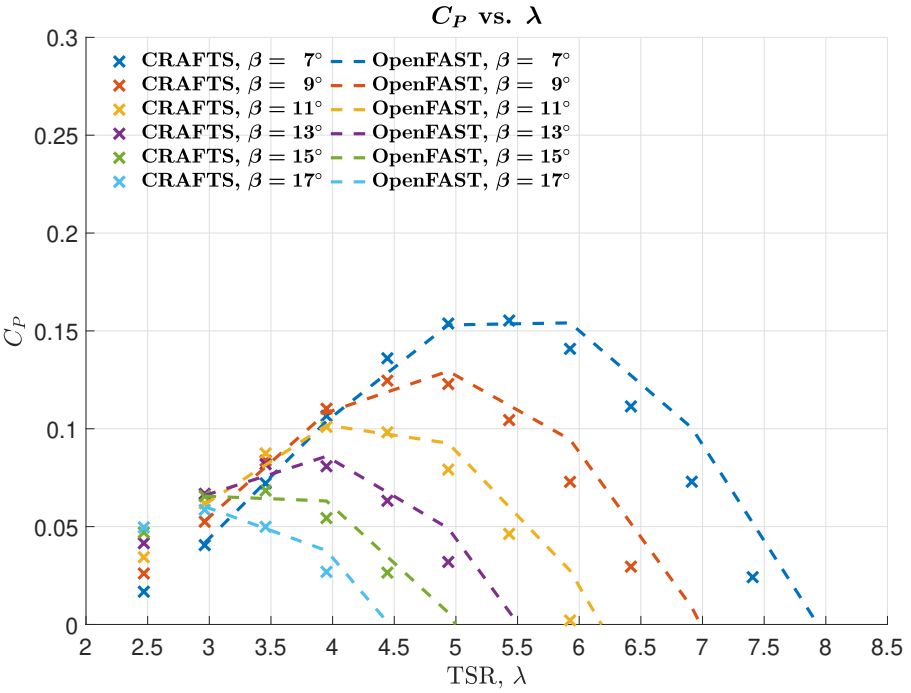

(b) C_P Vs λ for high pitch angles

Figure 5.5: Comparison Plots of C_P-λ between CRAFTS & OpenFAST

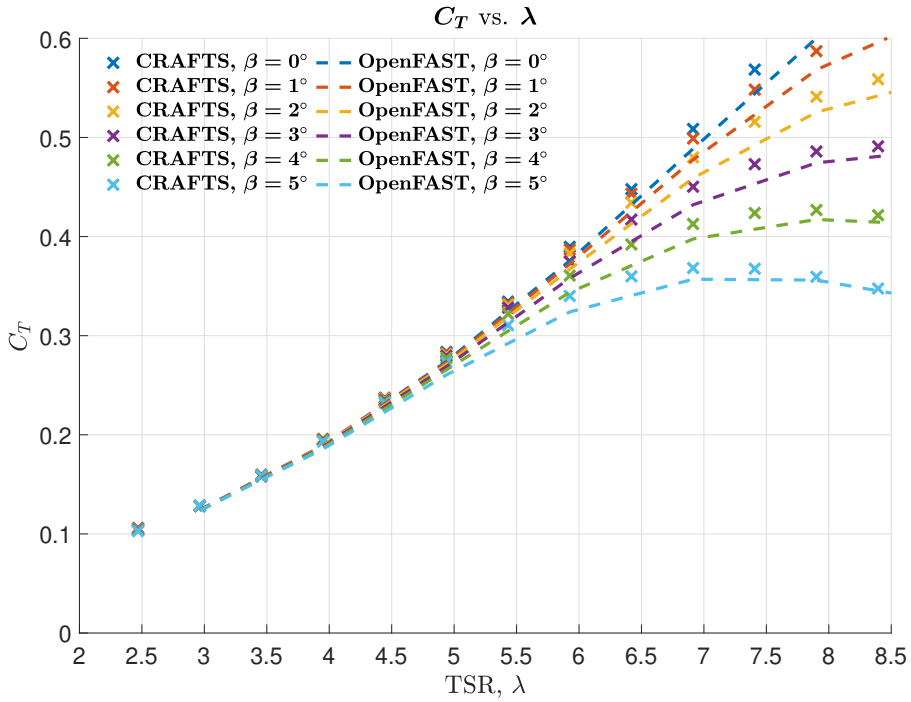

(a) C_T Vs λ for low pitch angles

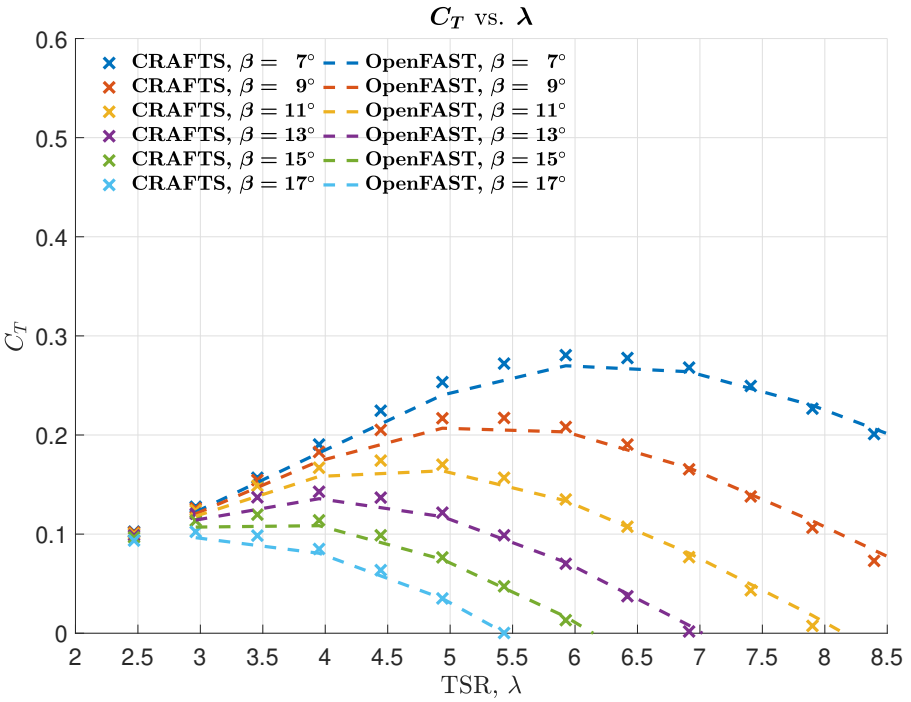

(b) C_T Vs λ for high pitch angles

Figure 5.6: Comparison Plots of C_T-λ between CRAFTS & OpenFAST

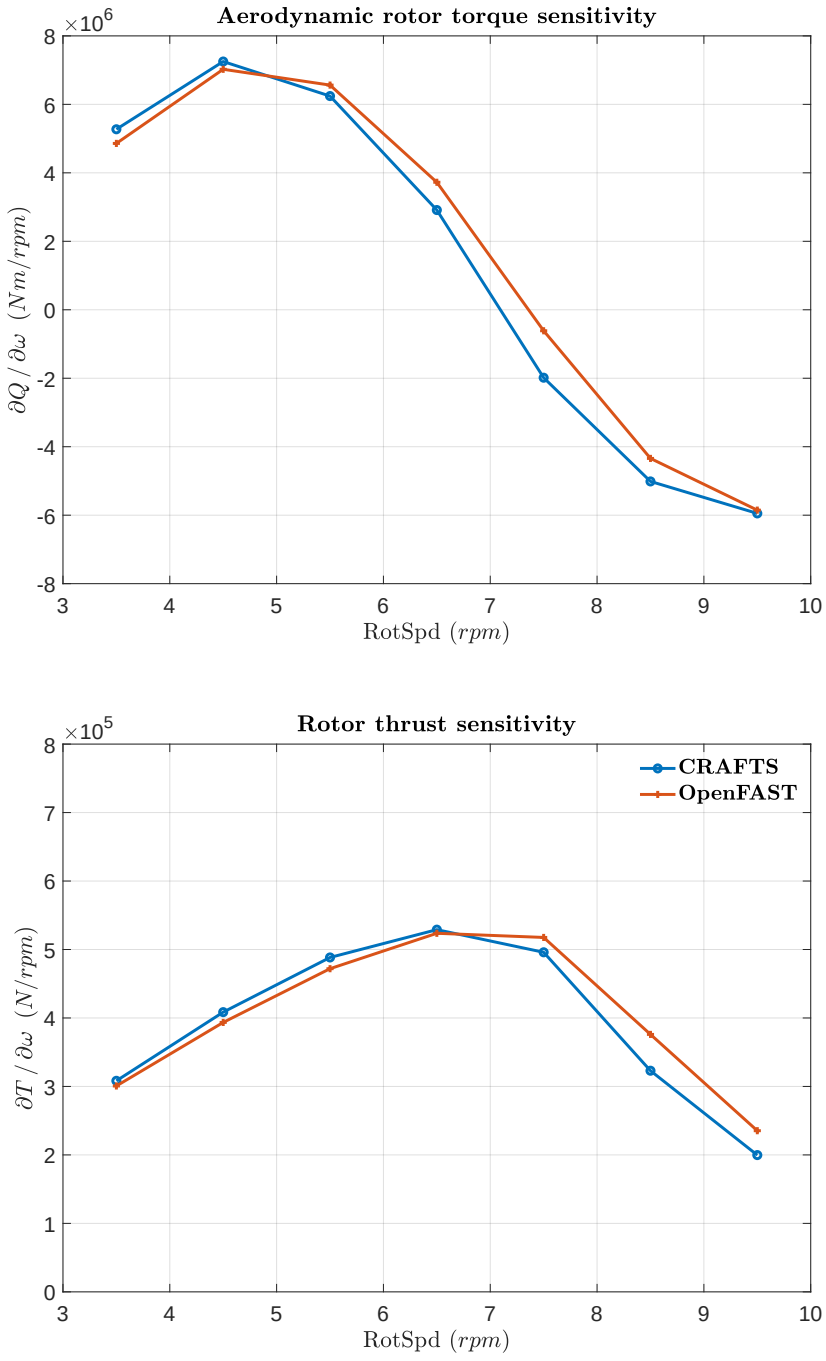

Figure 5.7: Sensitivity of torque and thrust w.r.t Rotor speed for TC 1.1

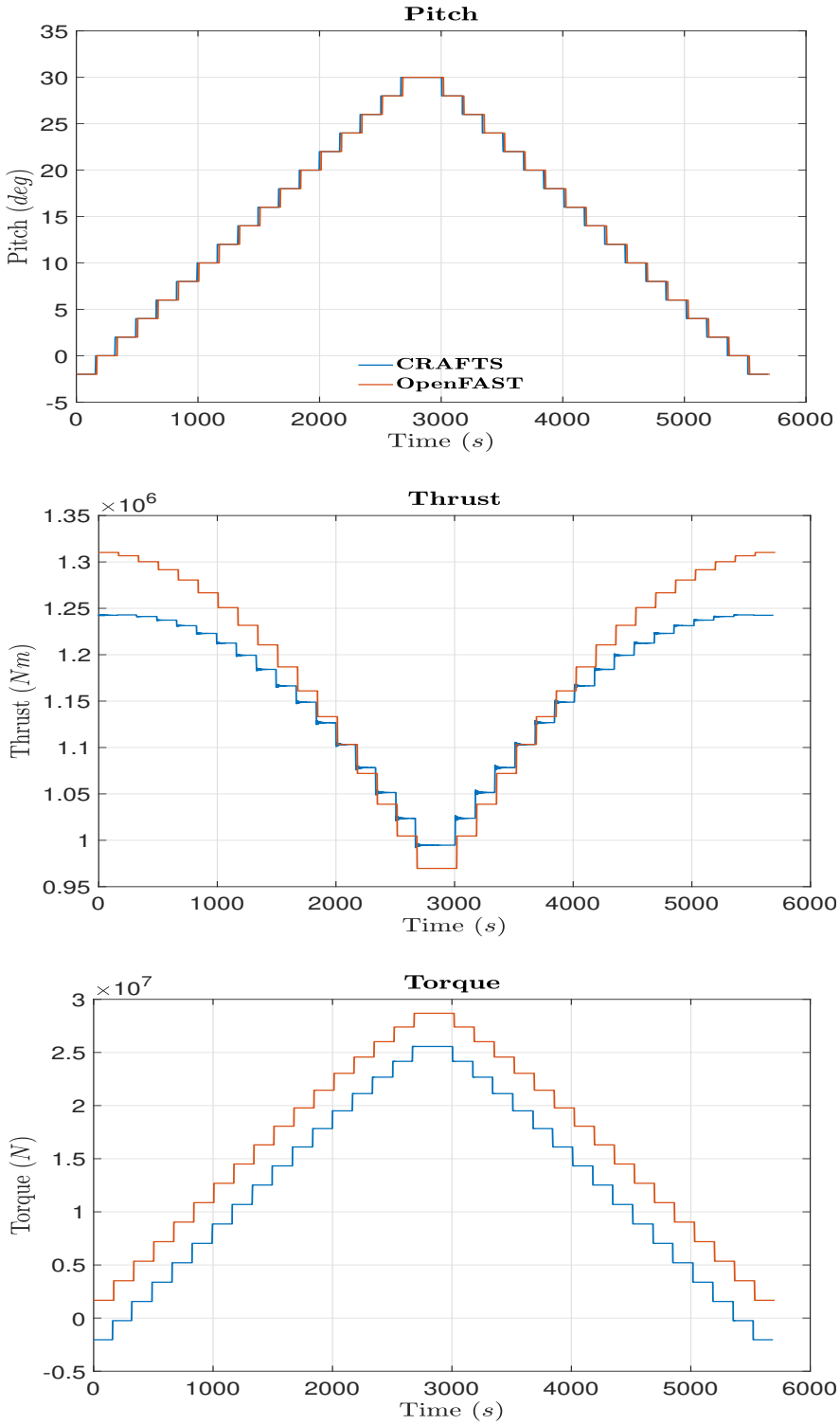

Figure 5.8: TC 2.1: $V_\infty = 27.69ms^{-1}$, Pitching Profile-Step

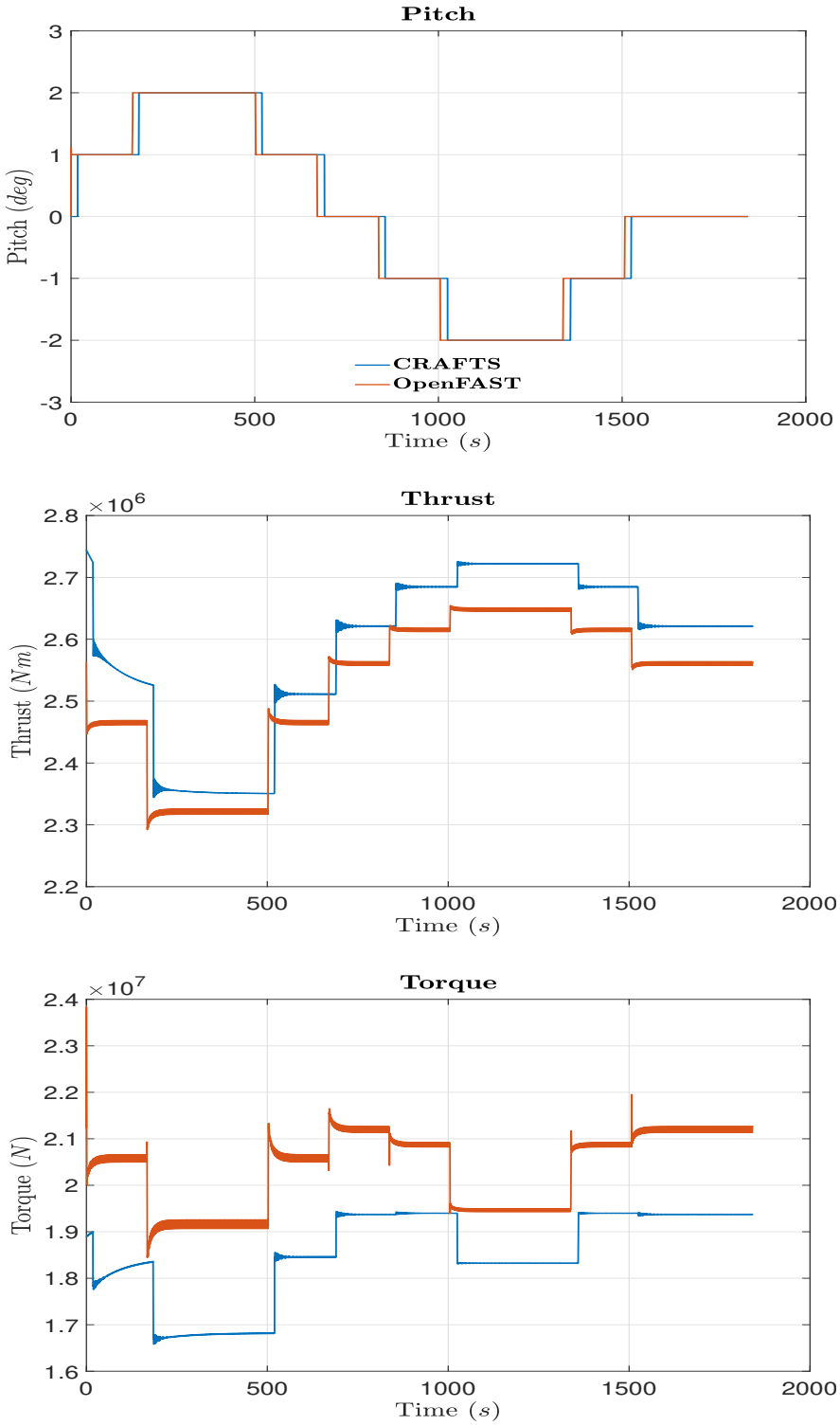

Figure 5.9: TC 2.2: $V_\infty = 12.83 ms^{-1}$, Pitching Profile-Step

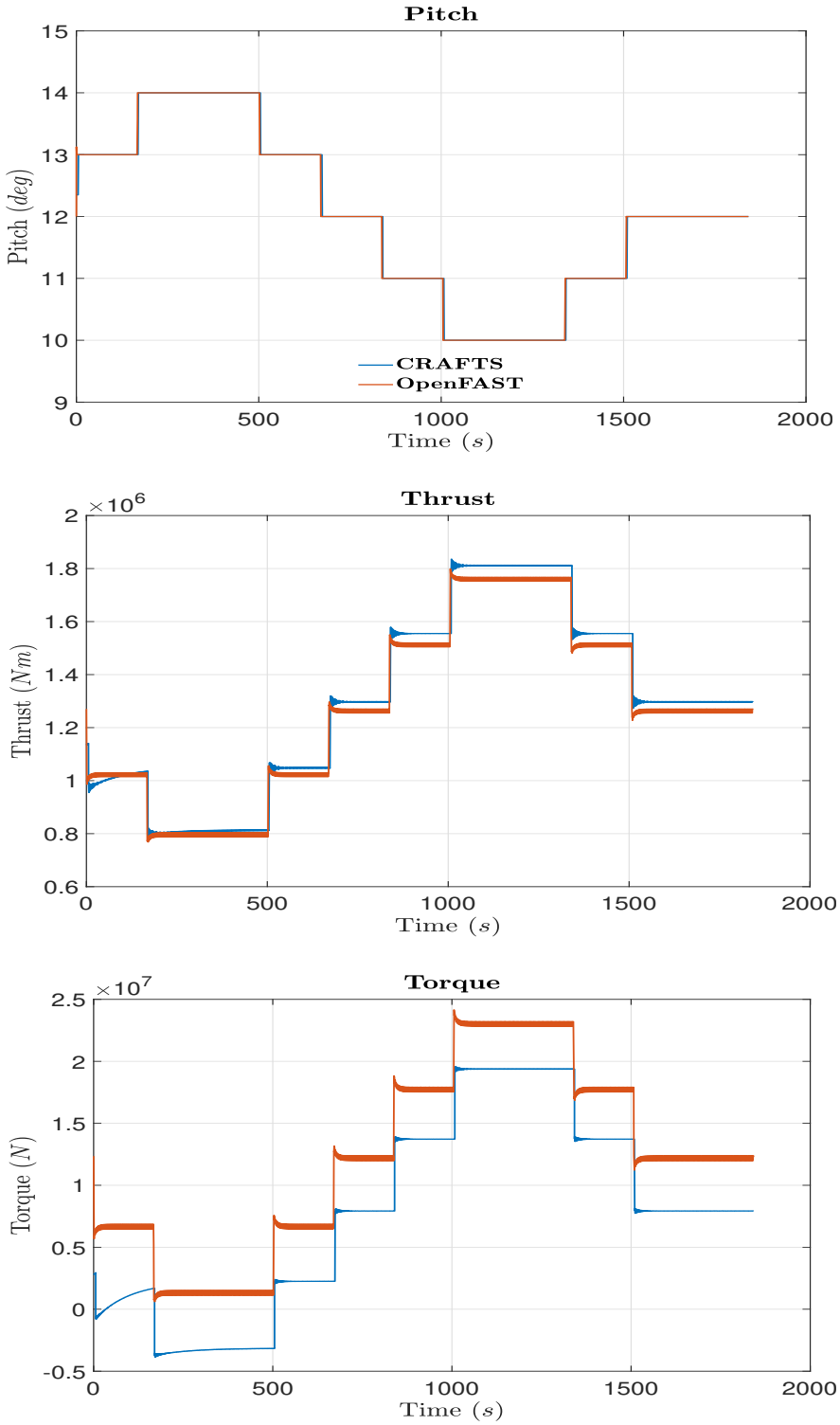

Figure 5.10: TC 2.3: $V_\infty = 18.41 ms^{-1}$, Pitching Profile-Step

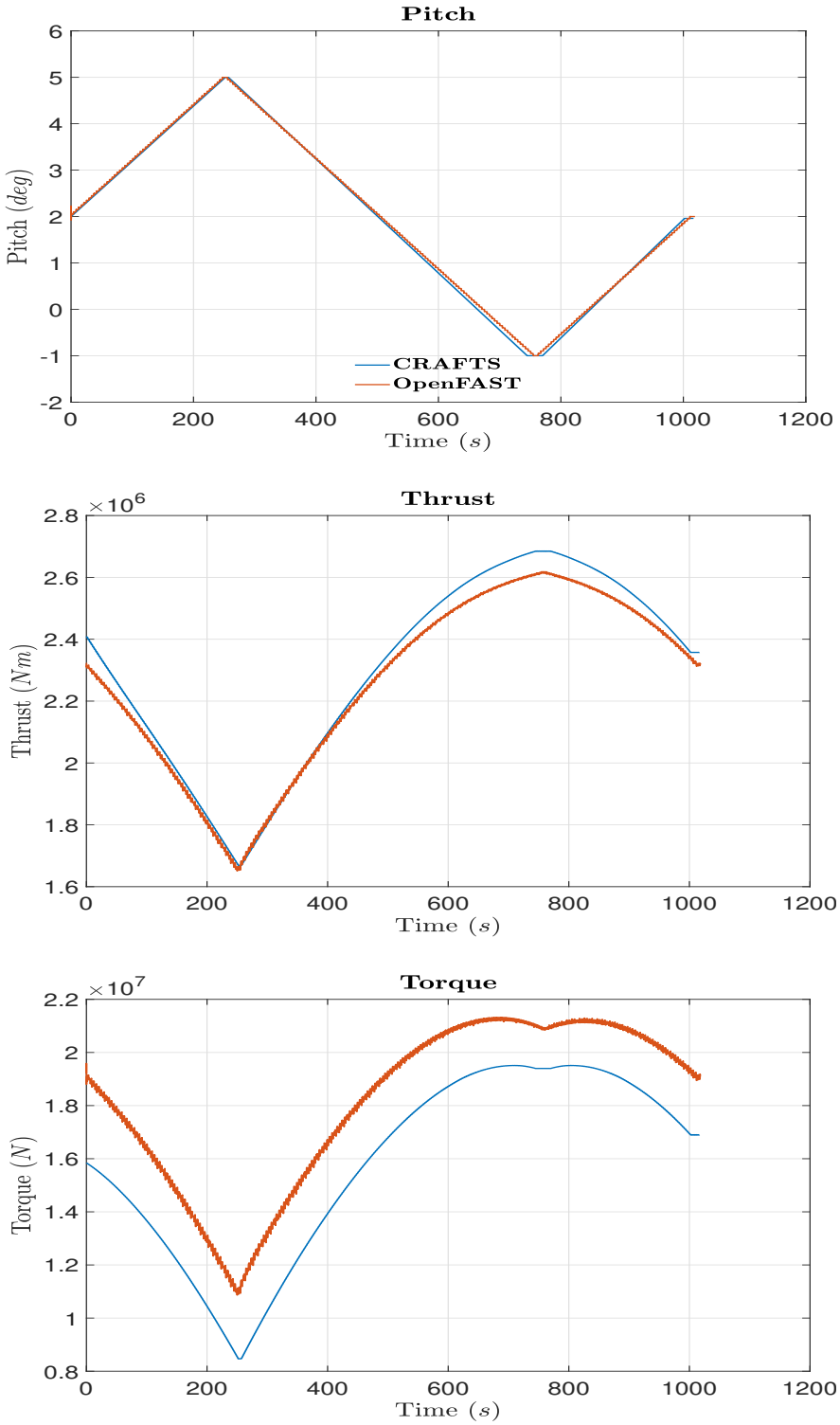

Figure 5.11: TC 2.4: $V_\infty = 12.83 ms^{-1}$, Pitching Profile-Ramp

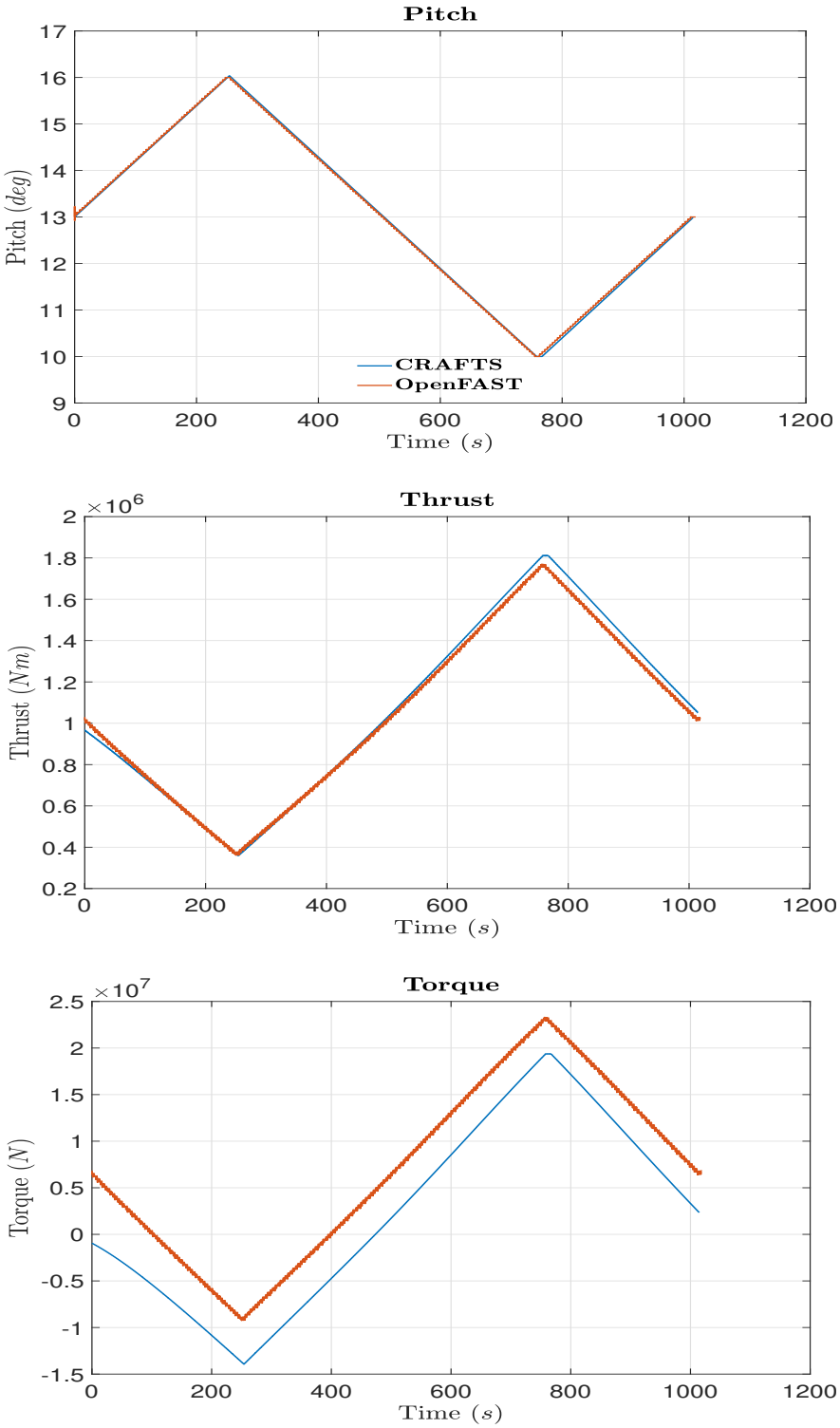

Figure 5.12: TC 2.5: $V_\infty = 18.41 ms^{-1}$, Pitching Profile-Ramp

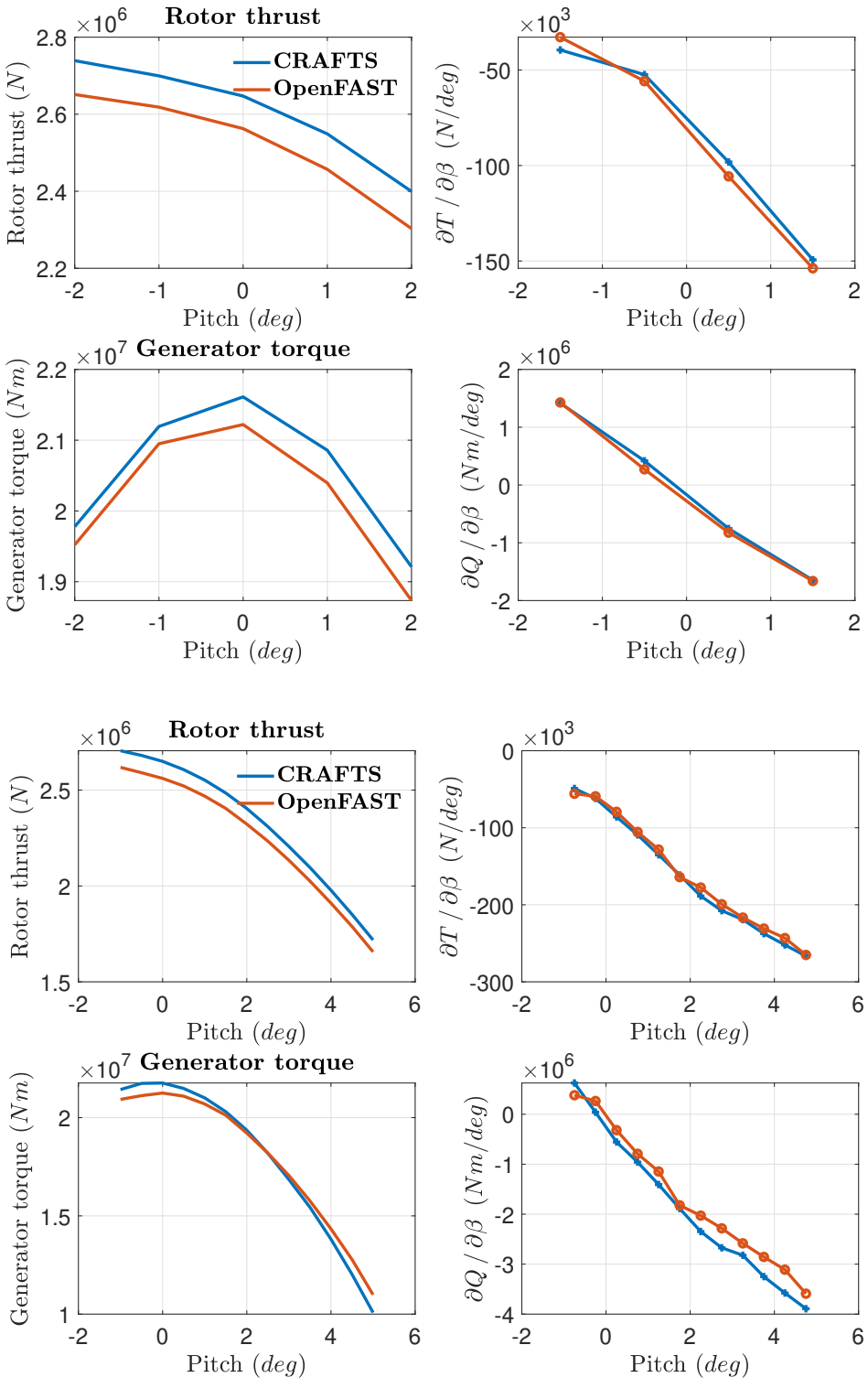

Figure 5.13: Sensitivity of thrust and torque to pitch angle

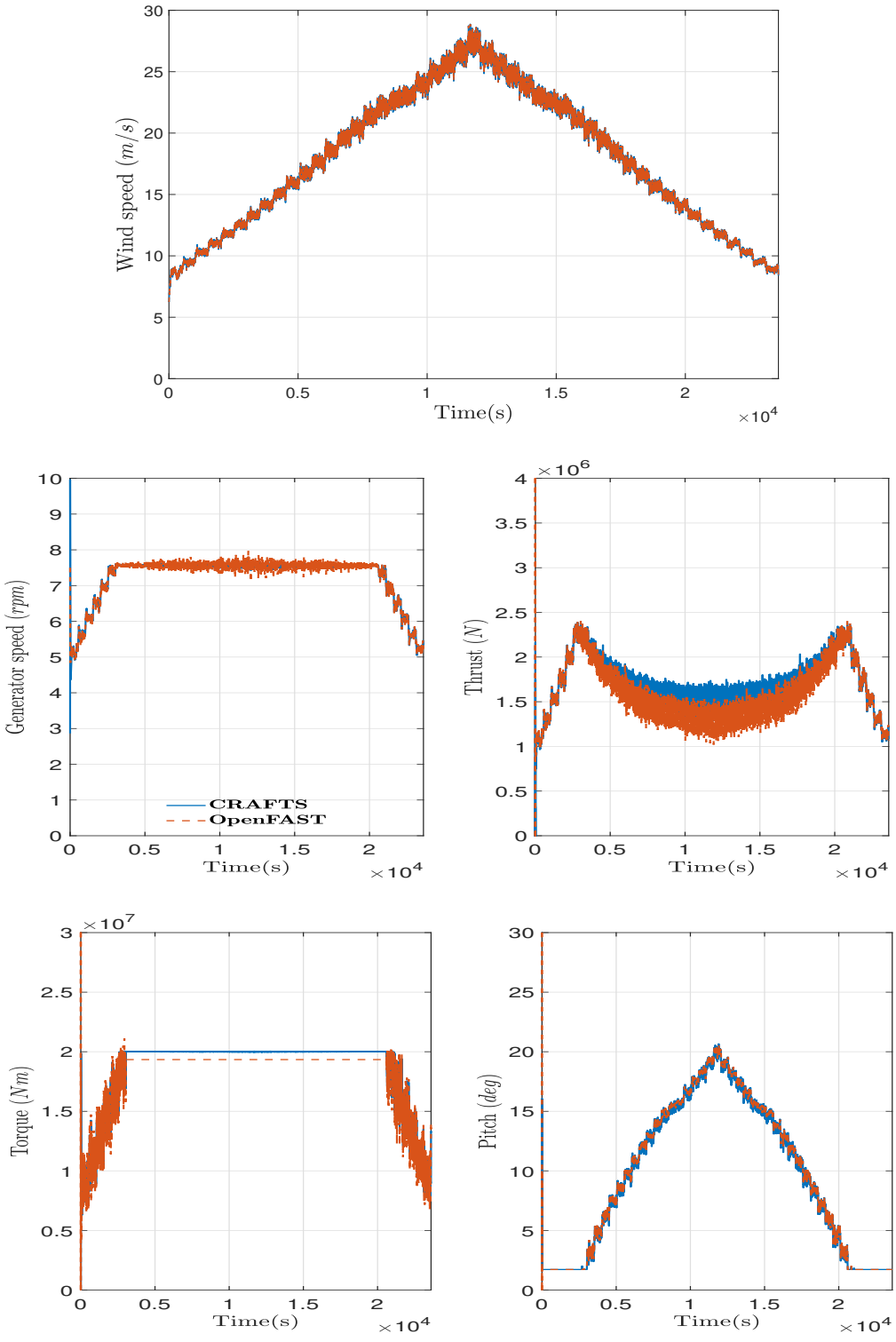

Figure 5.14: TC 3.1-Step wind profile: CRAFTS vs. OpenFAST

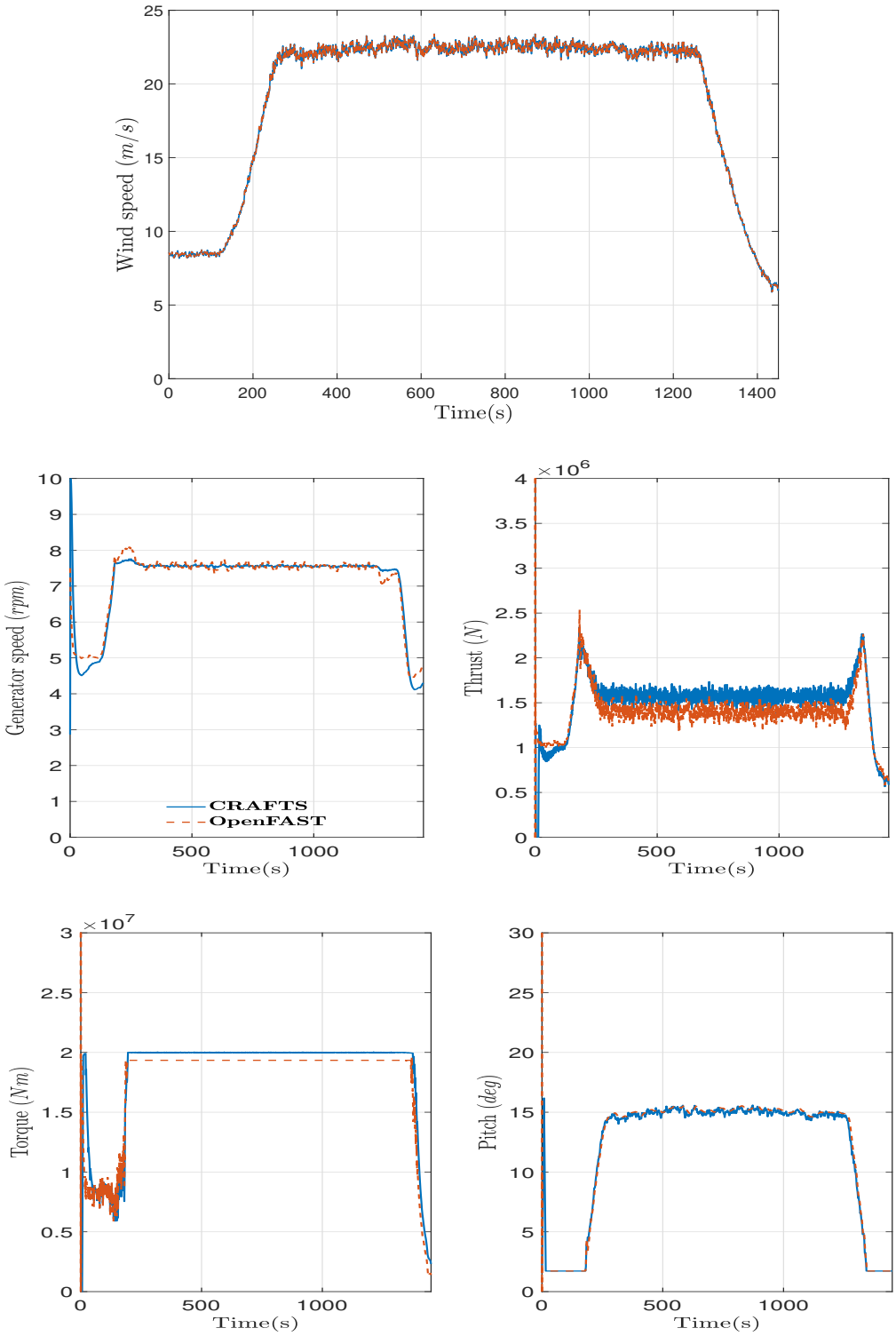

Figure 5.15: TC 3.2-wind gust: CRAFTS vs. OpenFAST

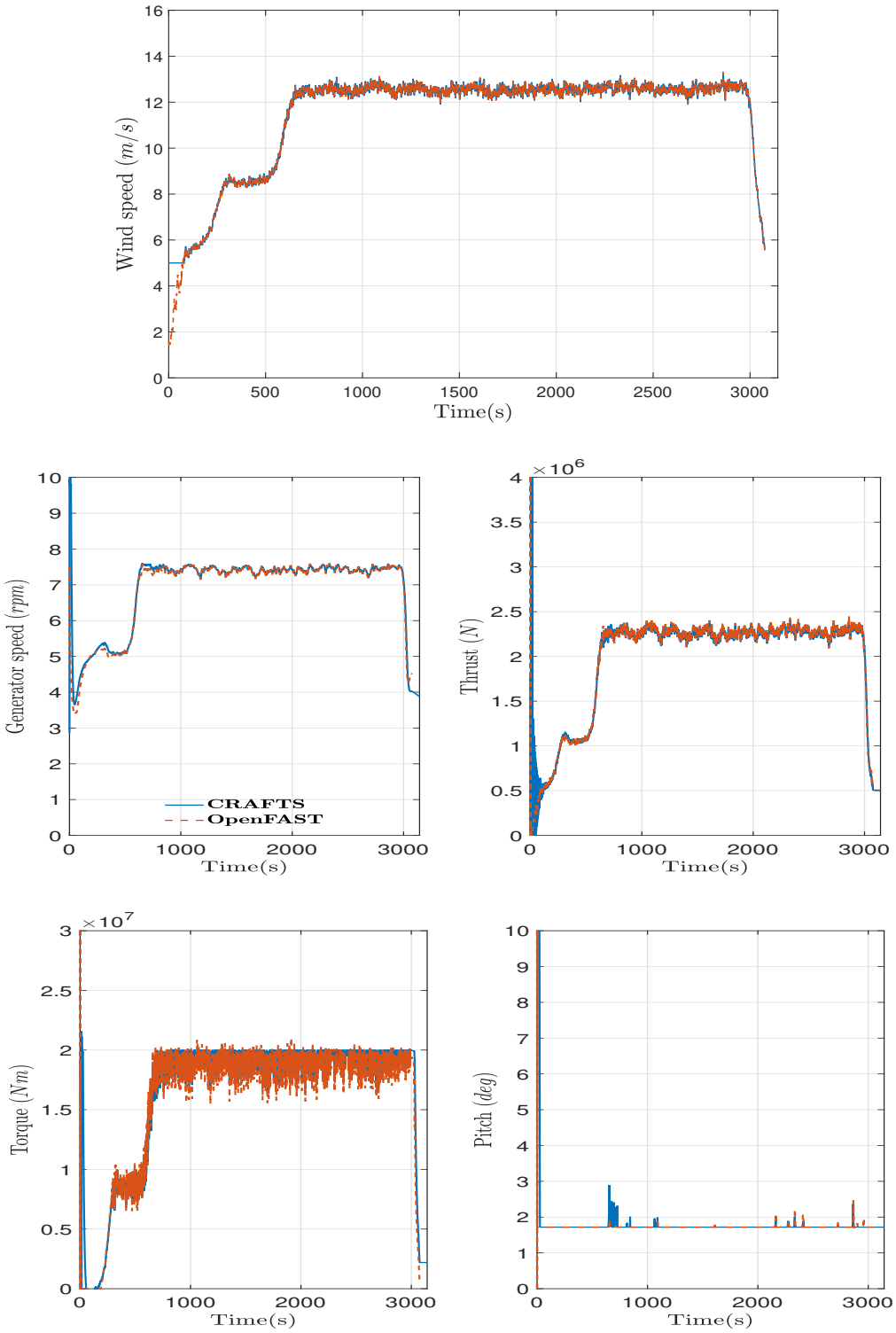

Figure 5.16: TC 3.3-Steady wind profile: CRAFTS vs. OpenFAST

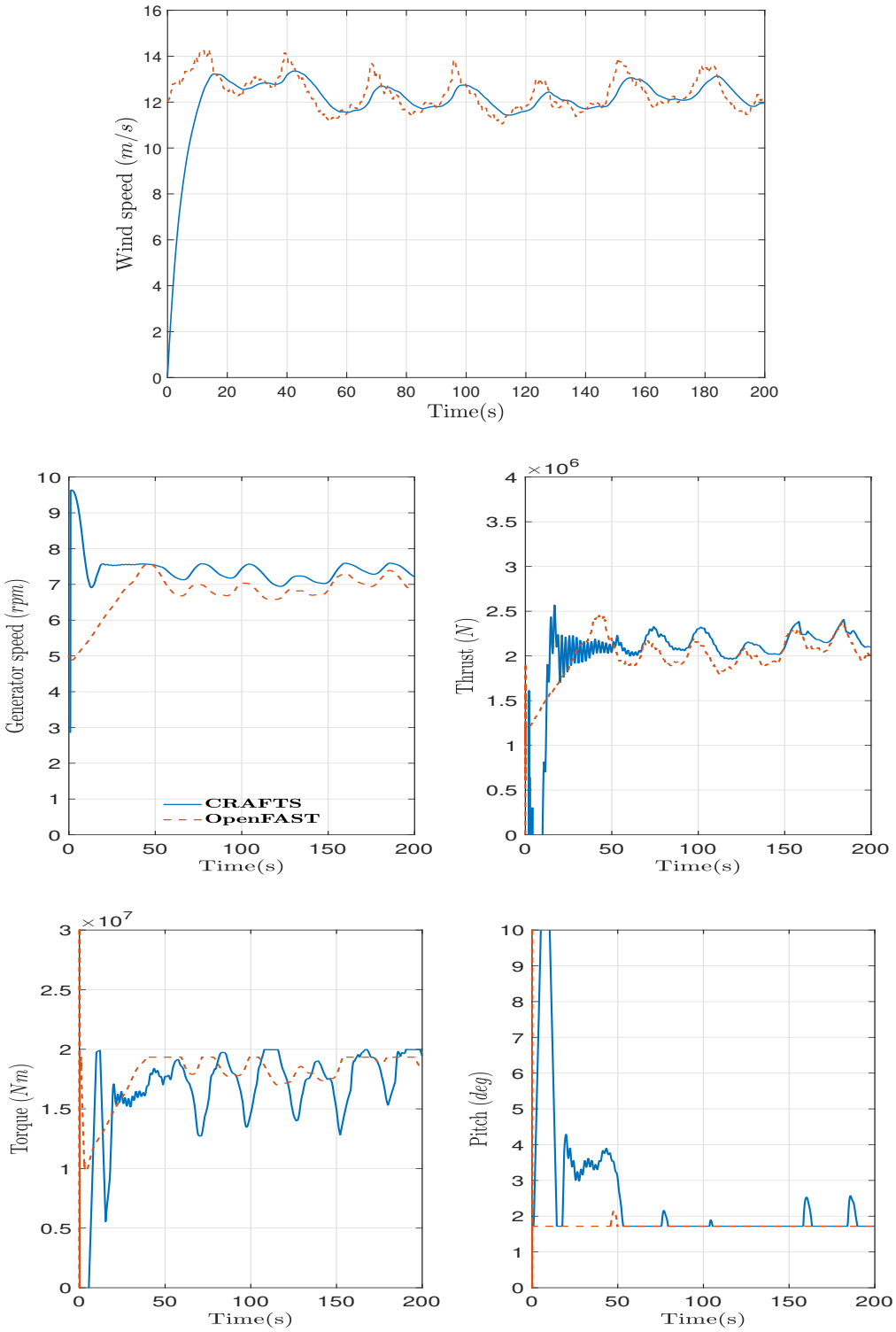

Figure 5.17: TC 3.4-Sinusoidal wind profile: CRAFTS vs. OpenFAST

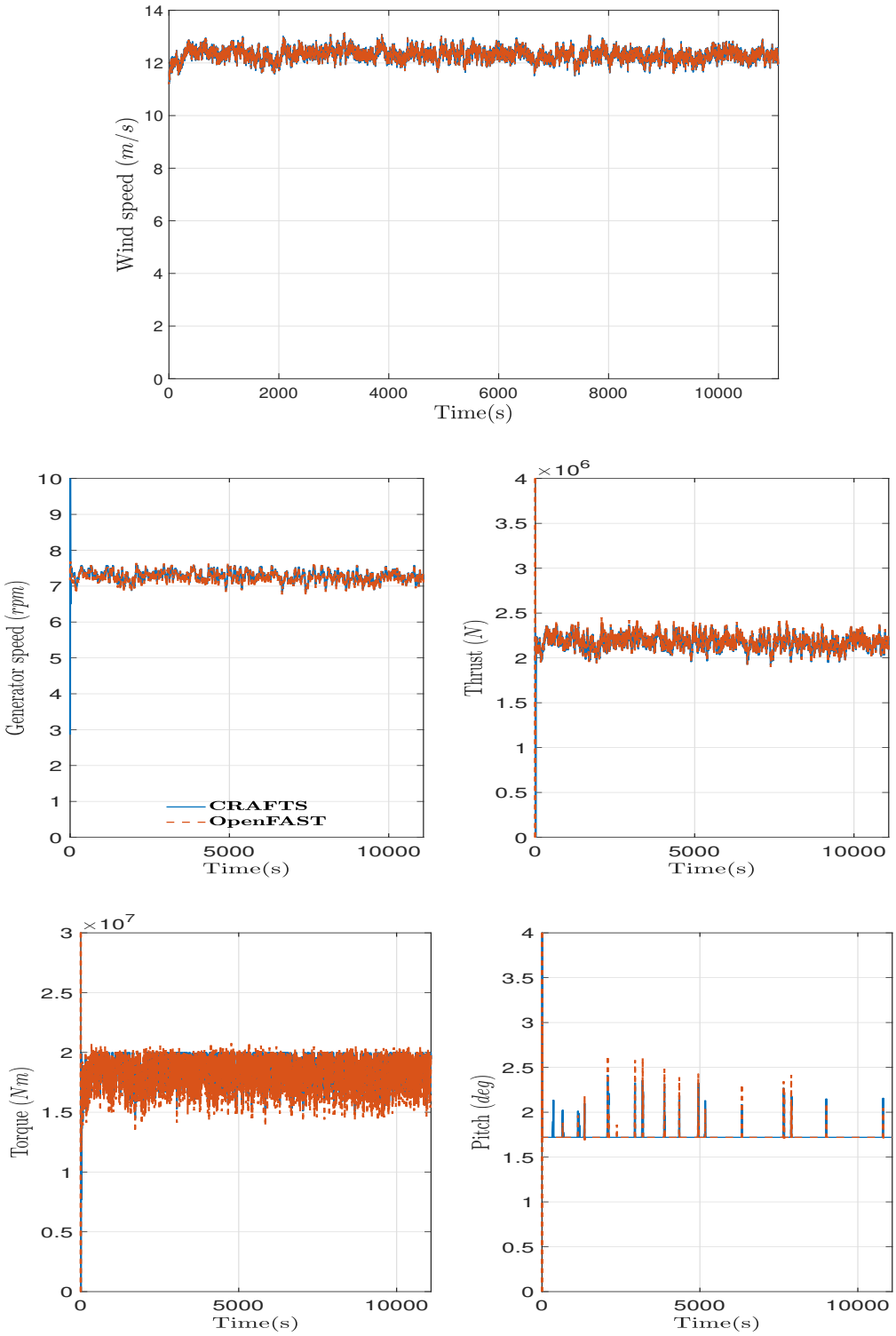

Figure 5.18: TC 3.5- wind spectral: CRAFTS vs. OpenFAST

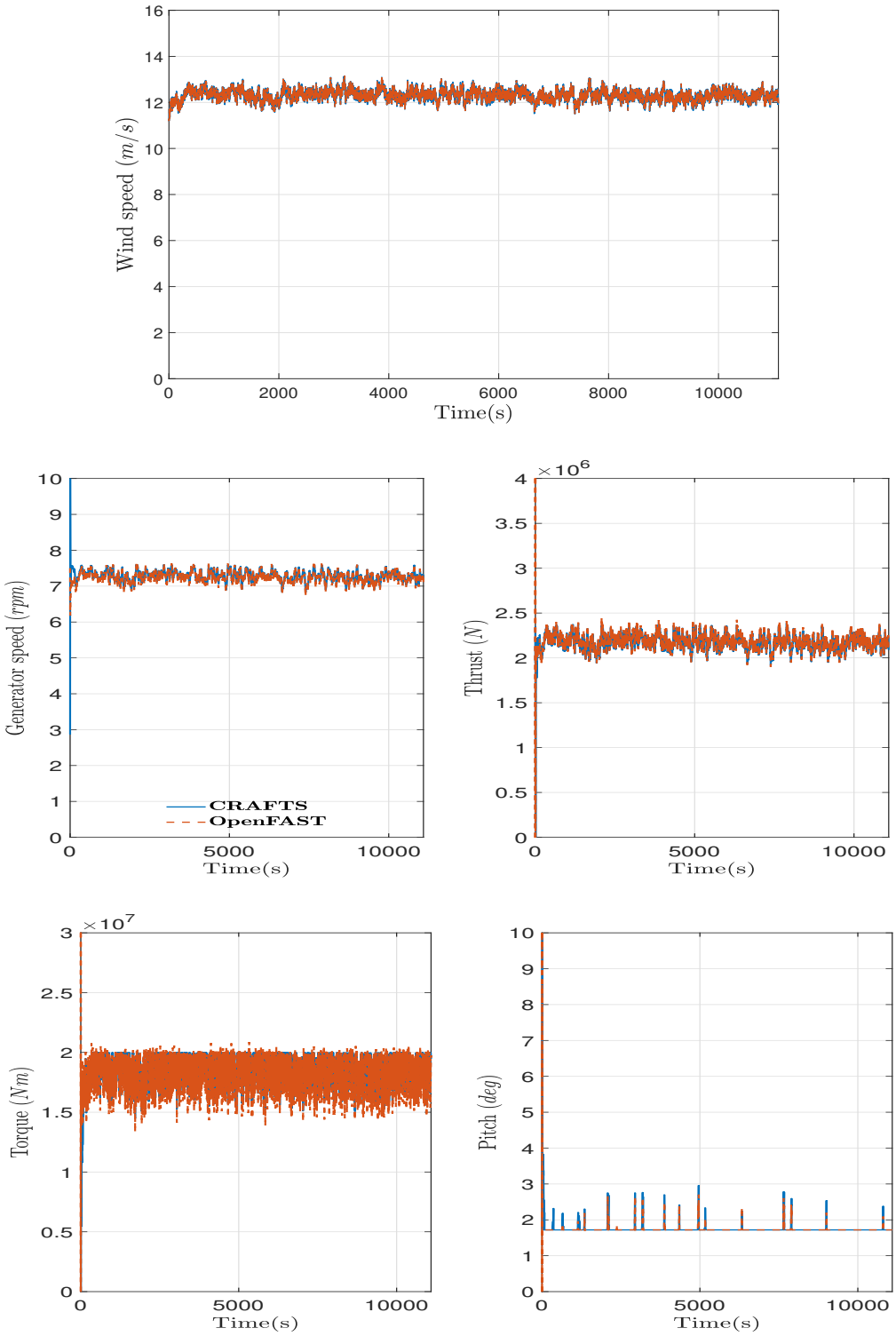

Figure 5.19: TC 3.6- wind spectral: CRAFTS vs. OpenFAST

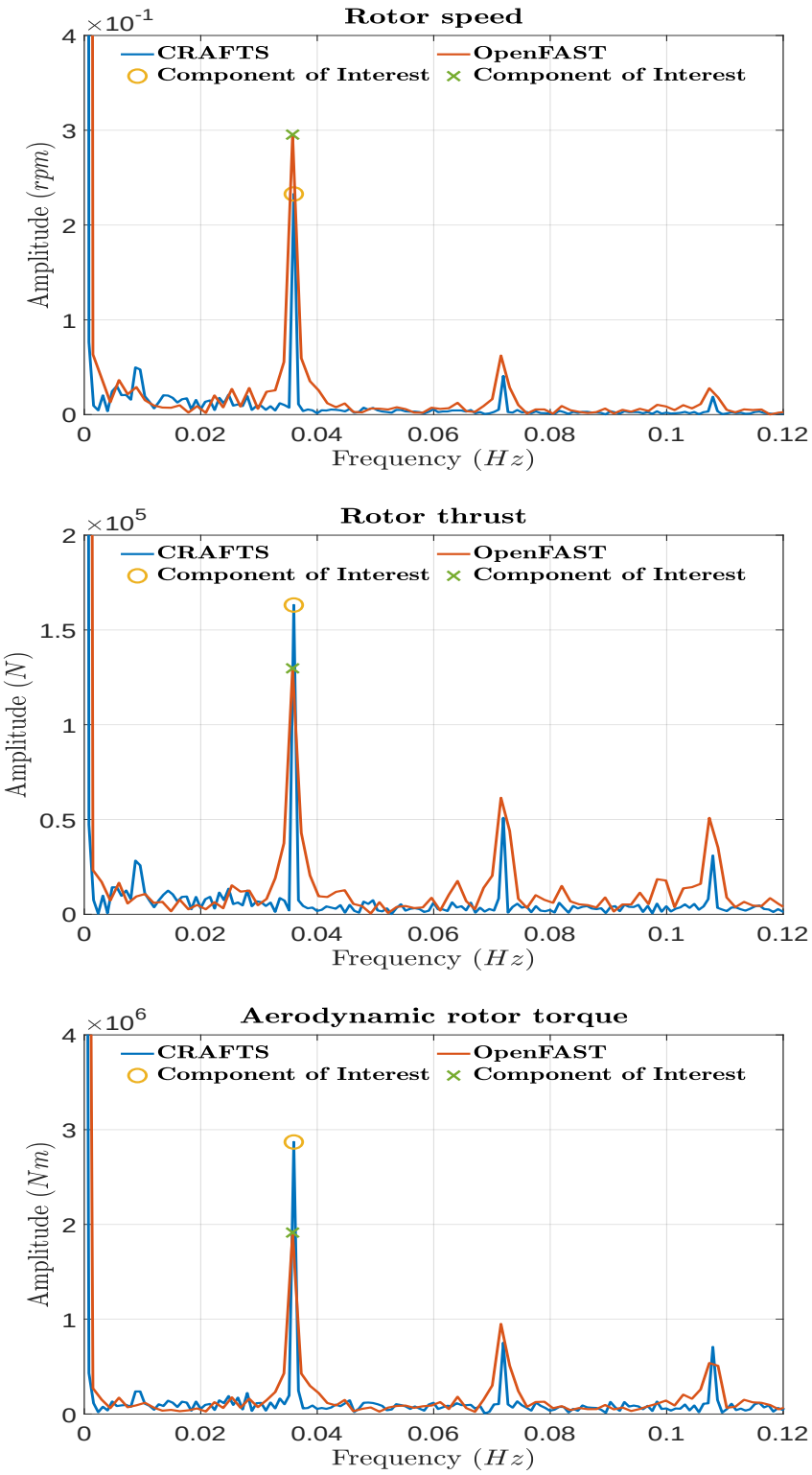

Figure 5.20: Frequency responses for rotor speed, thrust, and torque in TC3.4 (sinusoidal wind)

CHAPTER 6: NONLINEAR CONTROLLER EVALUATION

In this chapter, we present simulation data depicting the wind turbine's response to the nonlinear control approach under the same wind conditions as those encountered in TC 3.x. Fig. 6.2 to Fig. 6.6 provide a comparative view of the ROSCO and nonlinear controllers within TC 3.1-3.6. Furthermore, the time-domain characteristics of the generator speed in TC 3.2 is shown in Fig.6.7 whose findings are detailed in Table.6.1. Notably, both controllers exhibit remarkably similar performances. Though the performances of both the controller are quite similar but we can see some discrepancies in certain regions . For example in TC 3.1 & 3.2 shown in Fig. 6.2 & 6.3, when the control algorithm switches from regime 2 to regime 3 or vice versa we can observe some sharp peaks in aerodynamic thrust and pitching angle. Also from Fig. 6.4 to 6.6 , we can notice that in the transition region pitch angle command from both the controller are not exactly identical. We can attribute these issues with the absence of set-point smoother block in non-linear controller which we are planning to implement in our future work.

In our prior research conducted in [36], we have discussed the closed loop stability of the wind turbine in the operating regime of 2 and 3 in an theoretical manner. We have also developed common region of attraction between regime 2 & 3 where controller switches its control algorithm from regime 2 to regime 3, or vice versa. Brief procedure of finding these equilibrium points over entire operating region of the wind turbine is shown in an flowchart demonstrated in Fig.6.1.

We have determined these equilibrium points that were discussed in our previous research in the context of TC 3.1 (denoted by A, B, D, $D1$, and $D2$ in Fig.6.2 ,6.8 & 6.9). This visualization is an important step in the Lyapunov-based stability analysis of the wind turbine's equilibria. In regime 2, where power maximization is the main objective, the closed-loop system is asymptotically stable at the 2$^{\text{nd}}$ intersection from the left between the $C_p - \lambda$ curve and the $C_p = \left({}^{2k_t}/_{\rho A_{rotor} R^3}\right)(\lambda)^3$ curve,

Table 6.1: Time domain characteristics of the ROSCO and nonlinear controllers in TC 3.2 (Gust)

	Rise time(sec)	Peak time(sec)	Max.(%) overshoot	Settling time(sec)
ROSCO Controller	46	249.3	3.25	281.767
Non-Linear Controller	47.2	200	1.625	200

as proven by Johnson et al. [10]. These intersections can be seen in Fig. 6.2 as points D, $D1$, and $D2$. They correspond to stable equilibria at various rotor speeds and a blade pitch of 2^0 in regime 2.

In regime 3, the rated power is tracked by modulating the collective pitch angle while the wind turbine operates at sub-optimal rotor efficiency $C_p < C_{p,opt}$, which results in various equilibria corresponding to above-rated wind speeds, e.g. points A and B. These equilibria are obtained by drawing a horizontal line from the operating C_p across the $C_p - \lambda$ curve of the pitch angle β of interest, where the resulting 2^{nd} intersection point (i.e., points A and B in Fig. 6.8 denotes the stable equilibria, which is proven by Semrau et al. [36]. In Fig.6.8, $C_{p,e,1}$ and $\lambda_{E,1}$ correspond to the operating C_P and λ values for the equilibrium point A, whereas $C_{p,e,2}$ and $\lambda_{E,2}$ correspond to the operating C_P and λ values for the equilibrium point B.

Additionally, the transition between regime 2 and 3 is denoted by point D, where the generator torque of the two controllers remains at the same value. In Fig.6.9, $T_{g,max}$ denotes the maximum torque, and ω_{sw} indicates the switching speed. Regime 3 equilibria A, B, and D are distinct points on the $C_p - \lambda$ graph but they merge into one point in the $T_g - rpm$ graph. Similarly, D, $D1$, and $D2$ indicate the same point in the $C_p - \lambda$ graph but they separate into three points in the $T_g - rpm$ graph. The region before ω_{sw} in the $T_g - rpm$ graph is managed by the regime 2 controller and the region after ω_{sw} is managed by the regime 3 controller.

Regime-2 Equilibrium point determination:

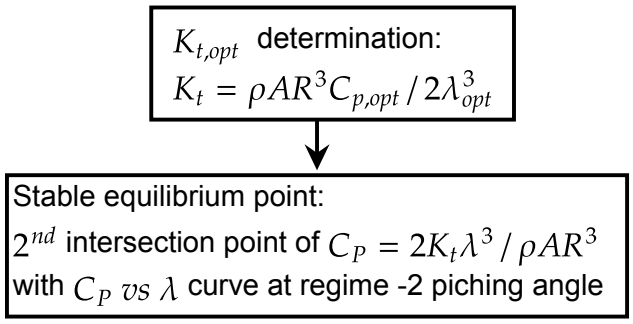

Regime-3 Equilibrium point determination:

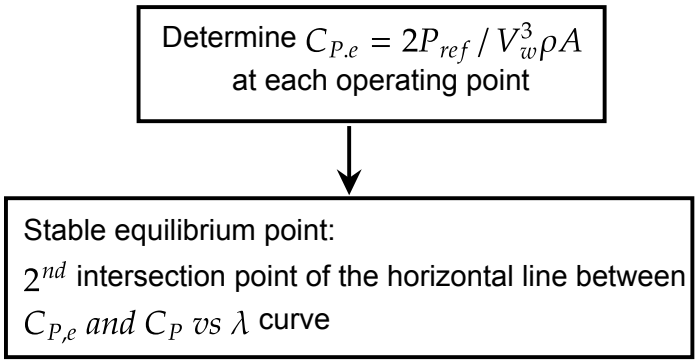

At switching point common Equilibrium point determination:

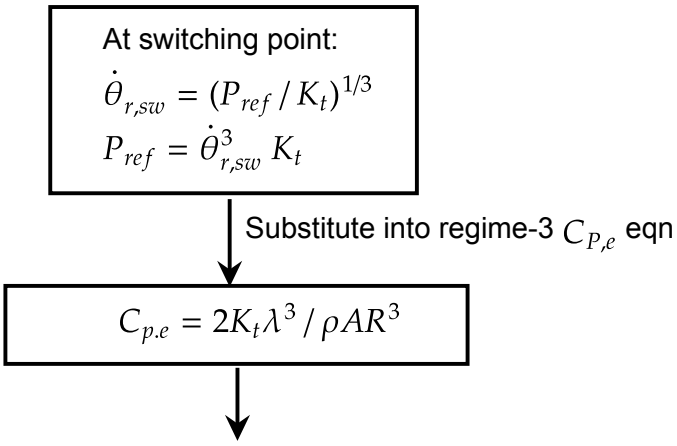

Which takes the same form as regime-2 resulting in a common equilibrium

Figure 6.1: Equilibrium point determination of the wind turbine

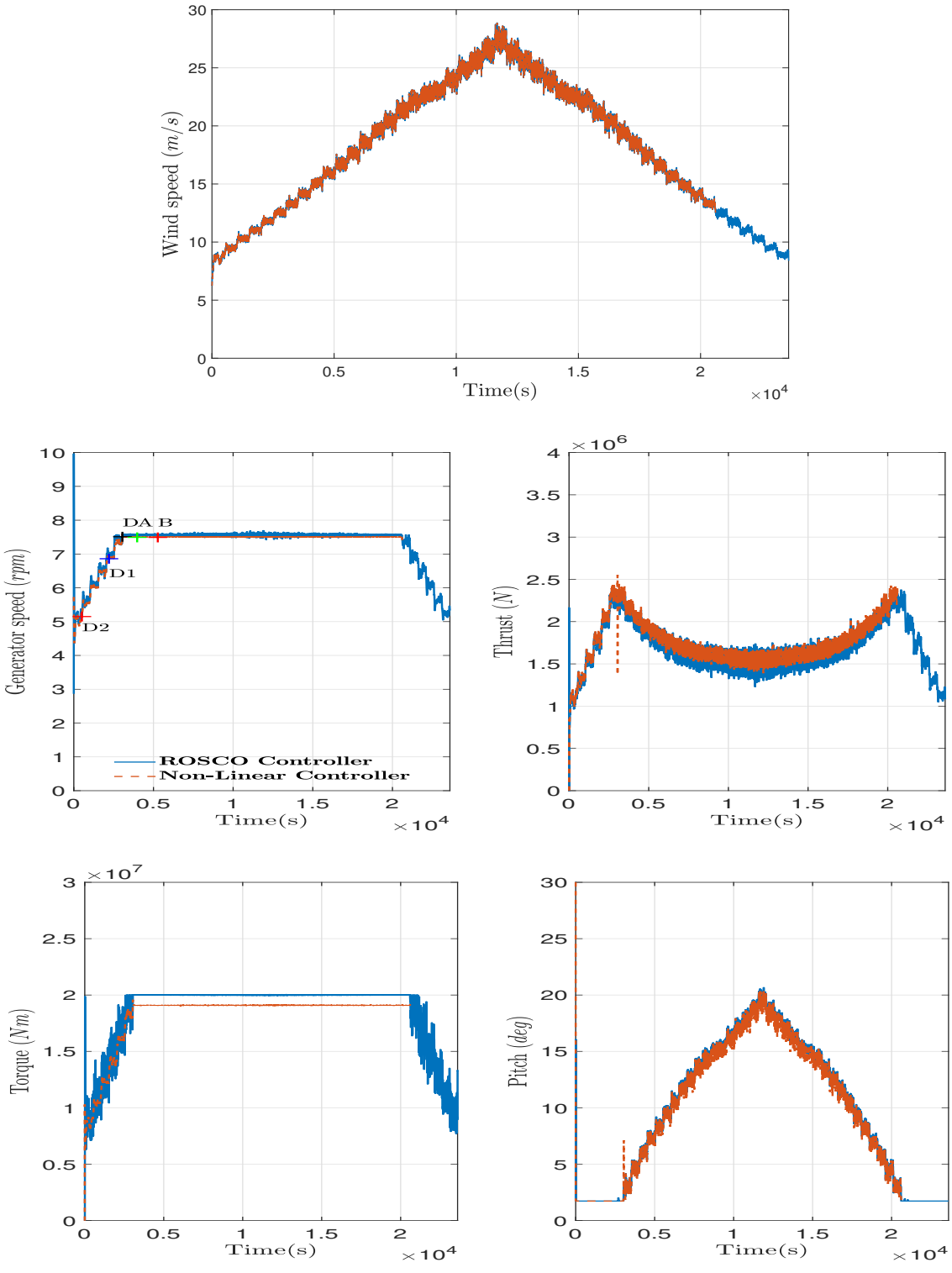

Figure 6.2: TC 3.1- Step wind profile: ROSCO vs. Non-linear Controller

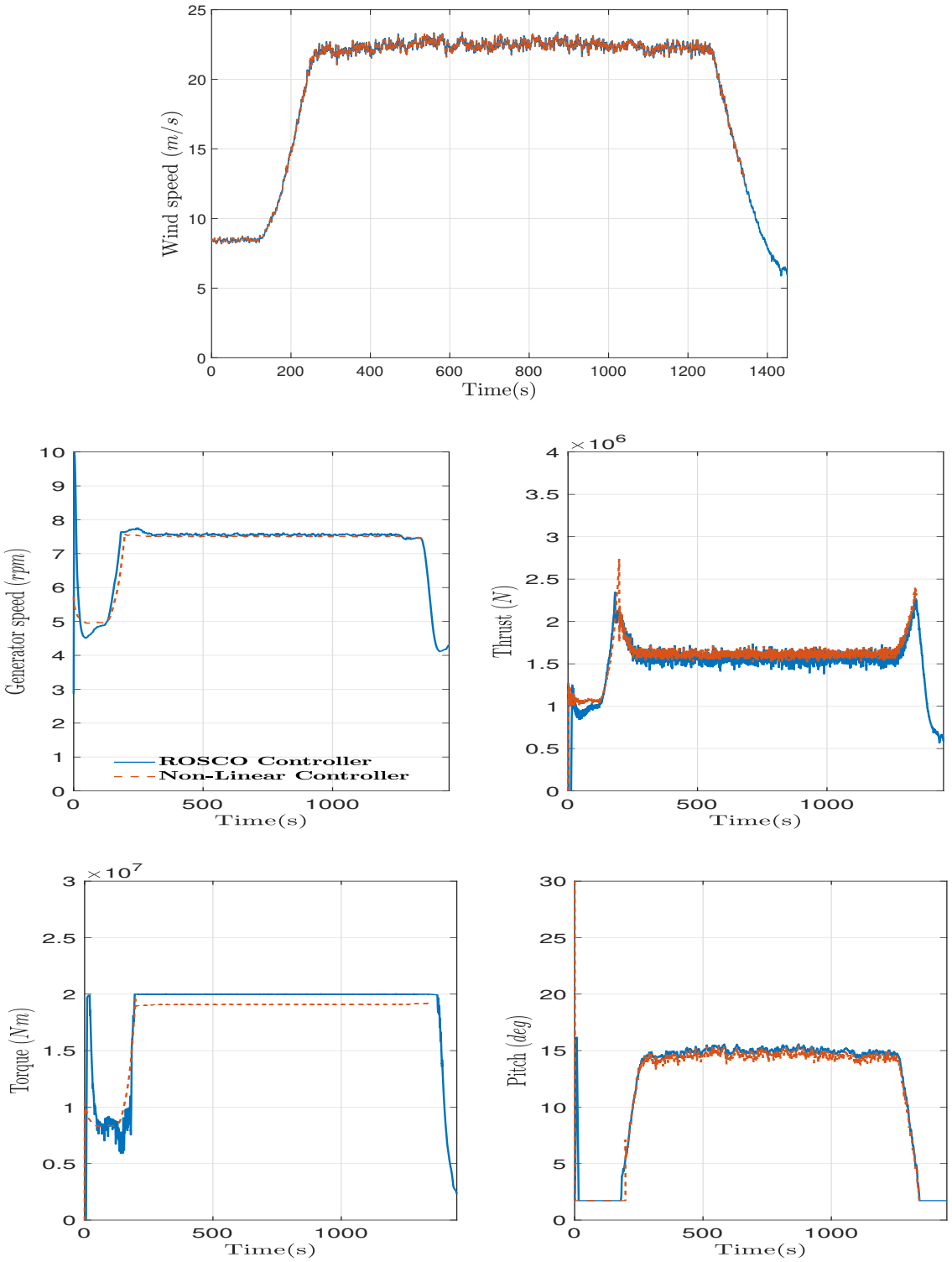

Figure 6.3: TC 3.2- wind gust: ROSCO vs. Non-linear Controller

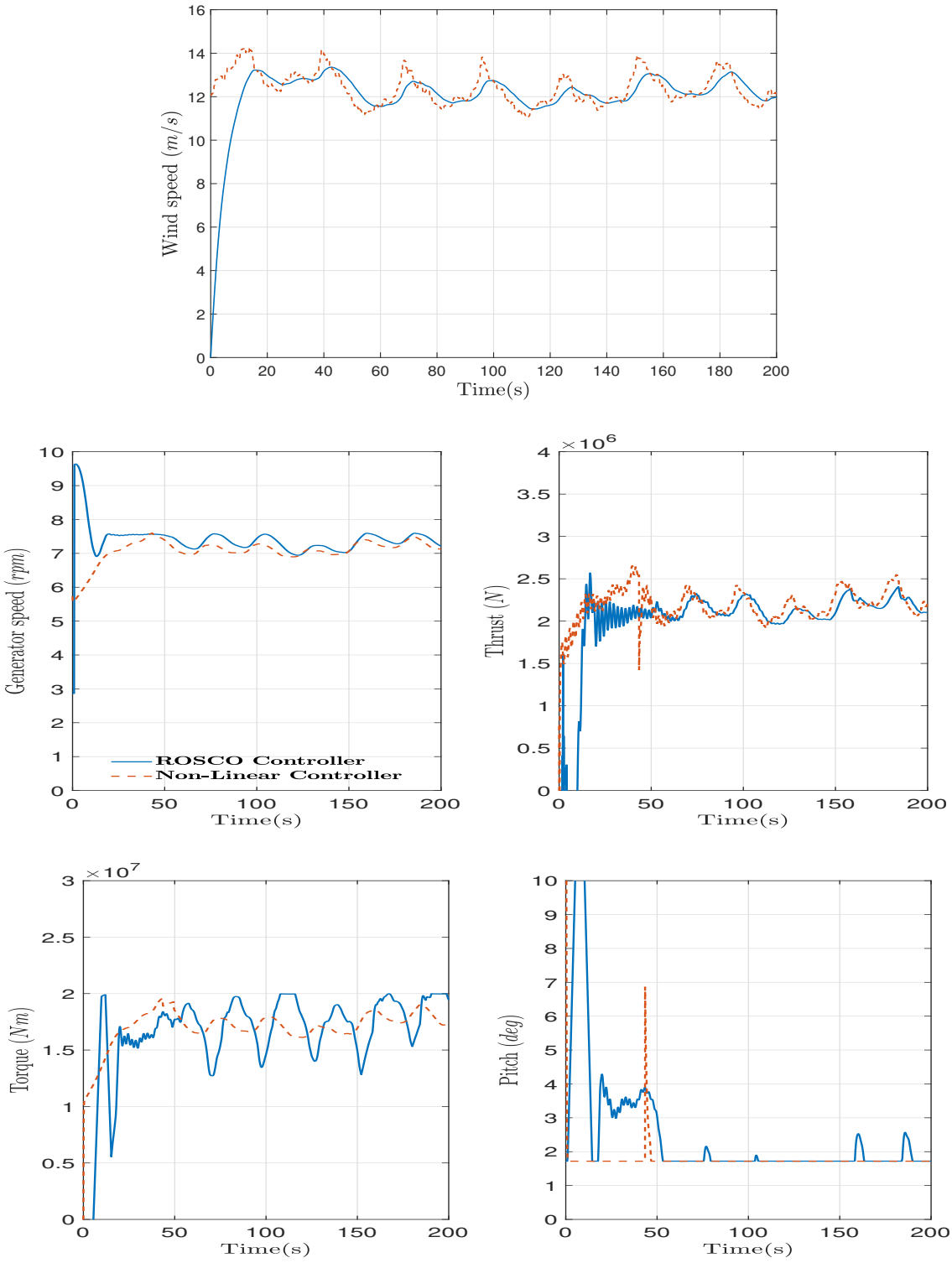

Figure 6.4: TC 3.4- Sinusoidal wind profile : ROSCO vs. Non-linear Controller

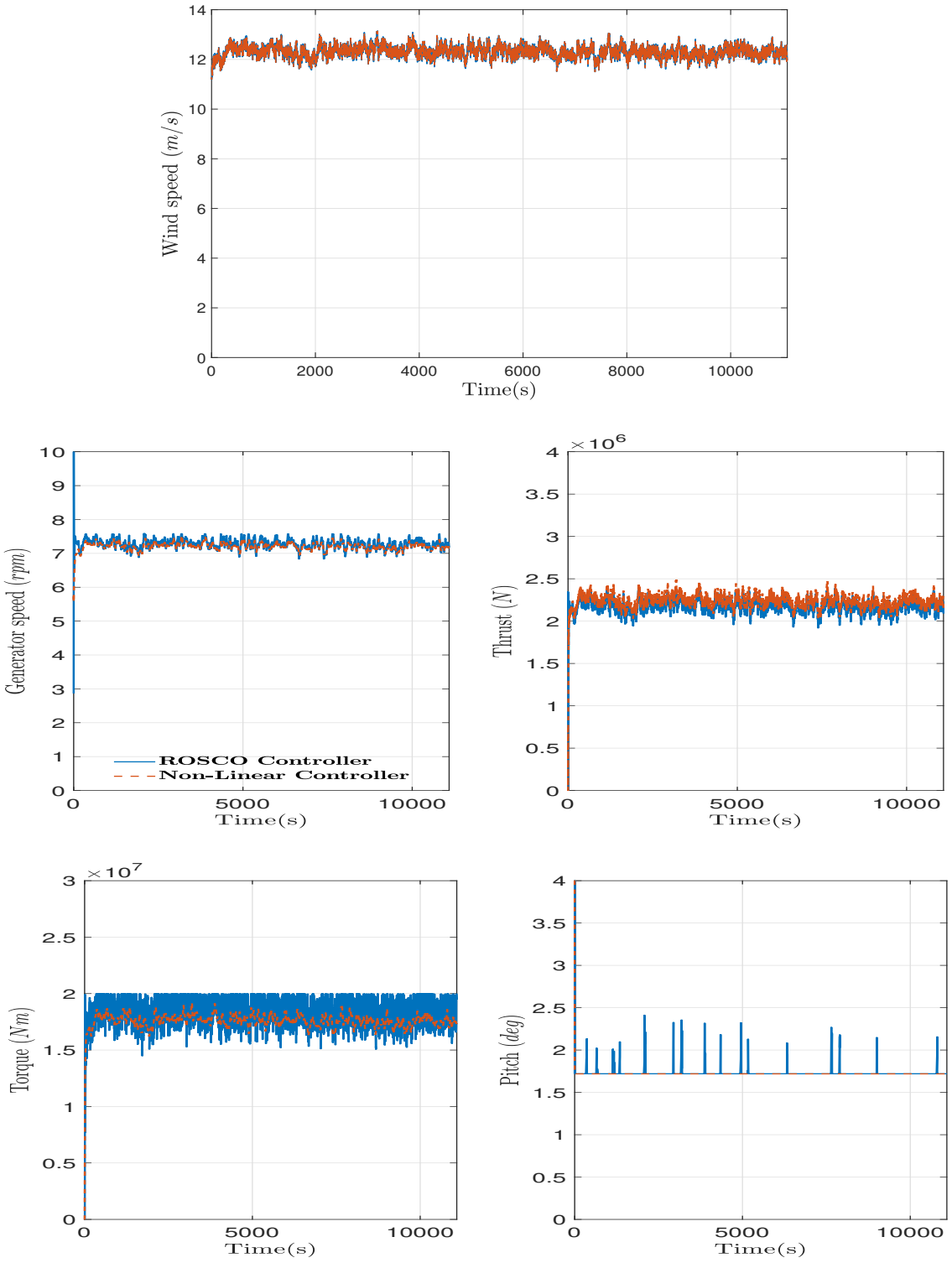

Figure 6.5: TC 3.5- wind spetral : ROSCO vs. Non-linear Controller

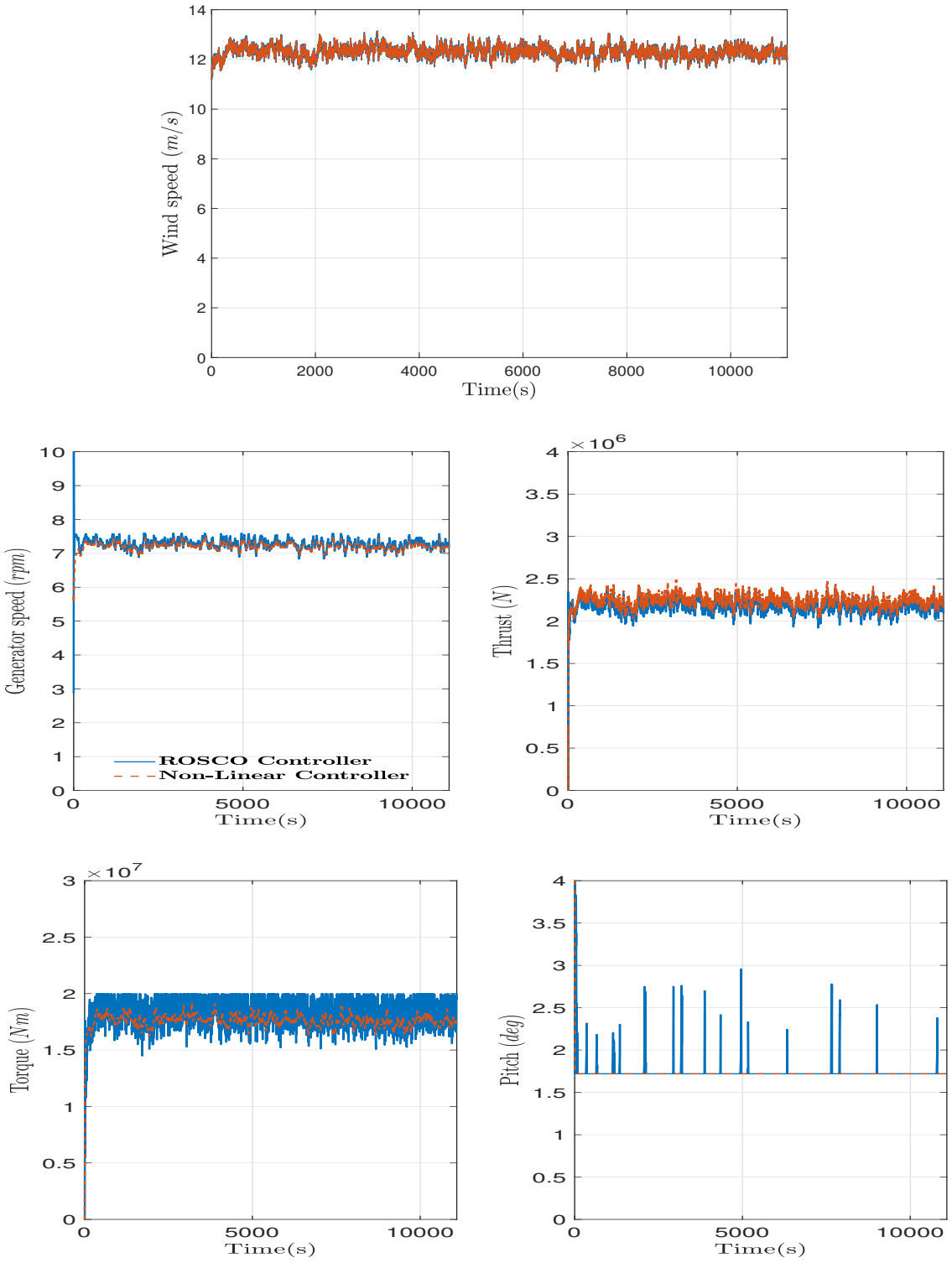

Figure 6.6: TC 3.6- wind spetral : ROSCO vs. Non-linear Controller

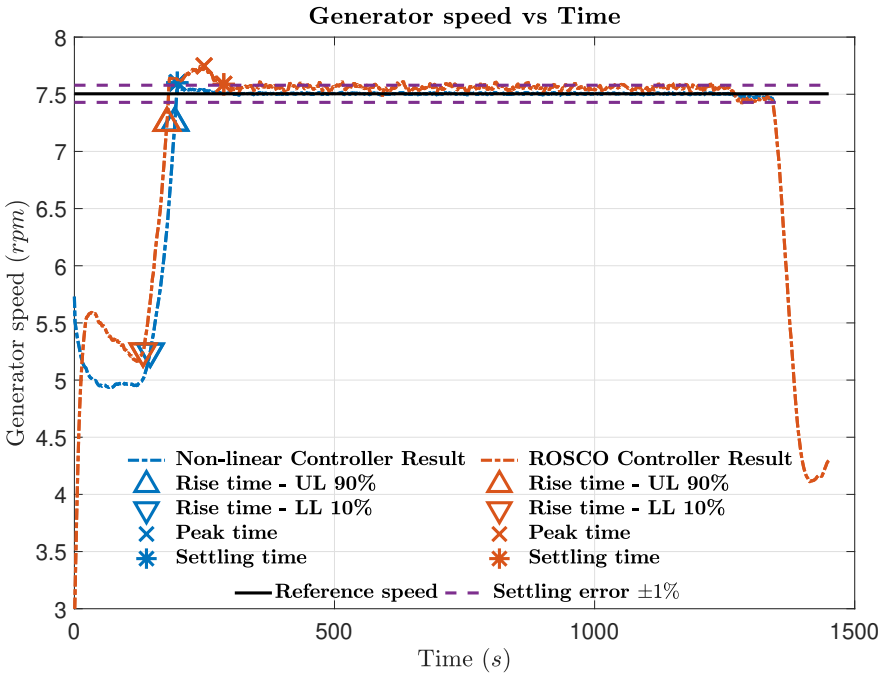

Figure 6.7: Time domain analysis - TC 3.2

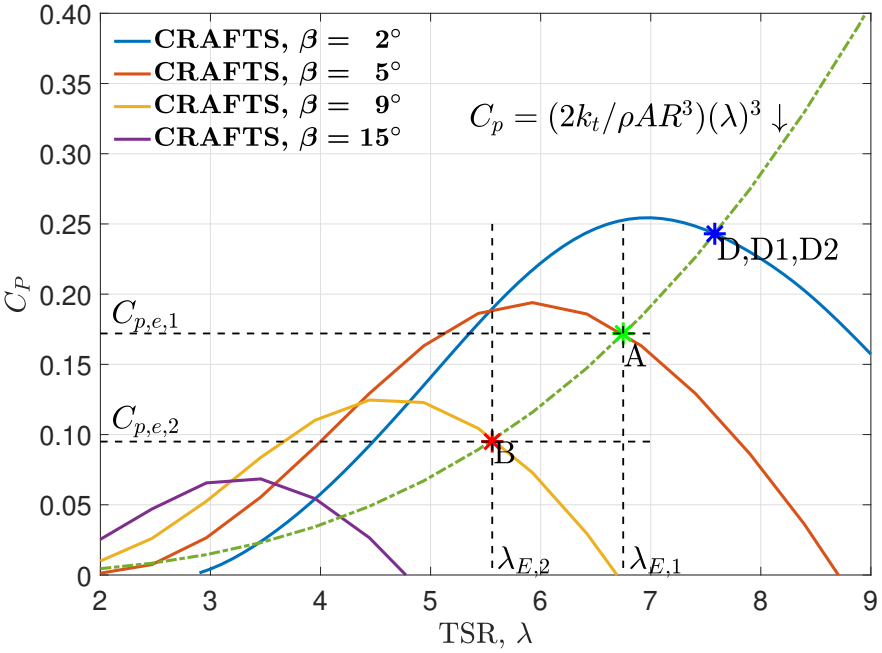

Figure 6.8: Equilibrium Points under β modulation for TC 3.1 (Stepped wind) w.r.to $C_p vs \lambda$ curve

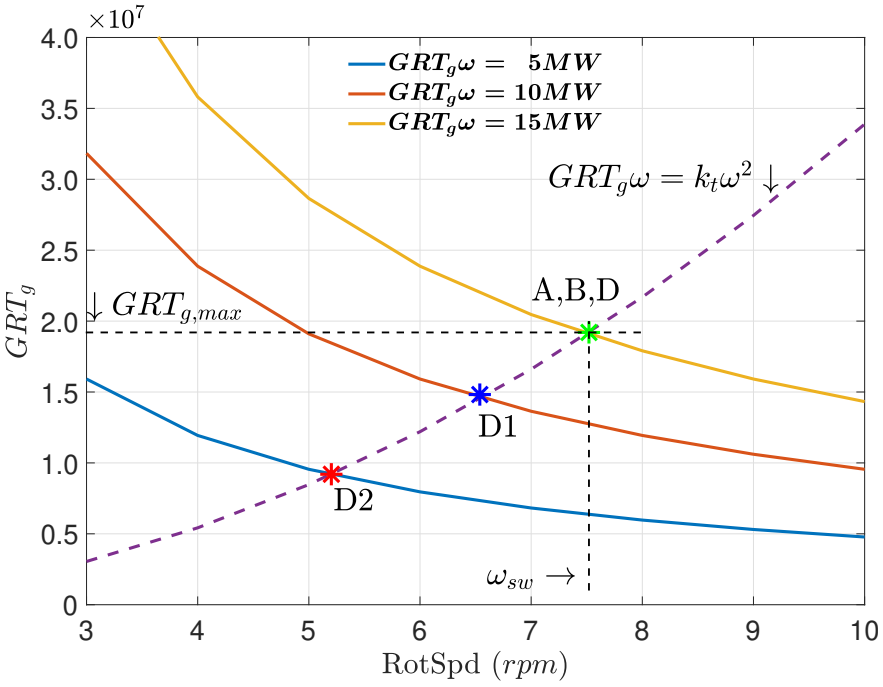

Figure 6.9: Equilibrium Points under β modulation for TC 3.1 (Stepped wind) w.r.to $T_g vs \omega$ curve

CHAPTER 7: CONCLUSION

The Control-oriented, Reconfigurable, and Acausal Floating Turbine Simulator (CRAFTS) represents a significant leap in the realm of wind turbine simulation. It introduces capabilities that were previously unreachable through traditional, low-fidelity methods. CRAFTS is not merely a simulation tool; it's a sophisticated system designed using a library-based, modular, and hierarchical model architecture. This unique architecture supports reconfigurability, allowing users to explore different wind turbine designs and control concepts with ease. Moreover, it seamlessly integrates nonlinear dynamics and multi-physics models, opening up possibilities for simulating a wide range of wind turbine variations. One of CRAFTS' notable features is its ability to engage in co-simulation with other numerical platforms, including the ROSCO toolbox in MATLAB. This feature extends CRAFTS' utility and its compatibility with other simulation and control tools in the wind turbine industry.

The validation of CRAFTS was carried out through multiple rigorous test cases in both open-loop and closed-loop conditions designed to compare its performance against industry-standard platforms like OpenFAST. In closed-loop condition, the standard ROSCO controller was applied to both CRAFTS and OpenFAST models, allowing a comprehensive evaluation. The results of the verification and validation analyses demonstrated that CRAFTS is more than capable of reproducing simulation outcomes similar to OpenFAST in various critical aspects. These include accurately representing aerodynamic forces, moments, torque, thrust and sensitivities of different aerodynamic aspects within the turbine.

Furthermore, CRAFTS shows its versatility and adaptability for control system designs by incorporating nonlinear controller developed in our prior research in CRAFTS model. This controller is designed to handle variable-speed wind turbines under a variety of operational conditions in an

non-linear manner and its asymptotic stability has been proved through previous research. The performance of this controller was rigorously evaluated across several closed-loop test cases with OpenFAST, showcasing CRAFTS' versatility.

Looking ahead, CRAFTS is poised for further advancements. Future developments will focus on expanding the library-based modules [42],[39], introducing features like individual pitch control, advanced hydrodynamics models, mooring actuation systems, and multi-variable robust control strategies. These enhancements will significantly augment CRAFTS' capability to model the dynamics of floating offshore wind turbines, incorporating control co-design approaches.

LIST OF REFERENCES

[1] U.S. Department of Energy Wind Market Reports: 2021 Edition. (https://www.energy.gov/eere/wind/wind-market-reports-2021-edition, Accessed January 21, 2022,2021)

[2] International Renewable Energy Agency Renewable Power Generation Costs in 2020. (https://www.irena.org/publications/2021/Jun/Renewable-Power-Costs-in-2020, Accessed January 21, 2022,2021)

[3] Jonkman, B., Mudafort, R. M., Platt, A., Branlard, E., Sprague, M., Jonkman, J., Hayman, G., Vijayakumar, G., Buhl, M., Ross, H., Bortolotti, P., Masciola, M., Ananthan, S., Schmidt, M. J., Rood, J., Mendoza, N., Hai, S. L., Hall, M., Sharma, A., Shaler, K., Bendl, K., Schuenemann, P., Sakievich, P., Quon, E.W., Phillips, M. R., Kusouno, N., Gonzalez Salcedo, A., Martinez, T., and Corniglion, R. OpenFAST/openfast: OpenFAST v3.1.0. (https://doi.org/10.5281/zenodo.6324288, Accessed September 08, 2022,2022)

[4] Lemmer, F., Yu, W., Luhmann, B., Schlipf, D. & Cheng, P. Multibody modeling for concept-level floating offshore wind turbine design. *Multibody System Dynamics*. **49**, 203-236 (2020)

[5] Petersson, J., Isaksson, P., Tummescheit, H. & Ylikiiskilä, J. Modeling and simulation of a vertical wind power plant in dymola/modelica. (Linköping University Electronic Press,2012)

[6] Eberhart, P., Chung, T., Haumer, A. & Kral, C. Open source library for the simulation of wind power plants. (Linköping University Electronic Press,2015)

[7] Leimeister, M., Kolios, A. & Collu, M. Development and Verification of an Aero-Hydro-Servo-Elastic Coupled Model of Dynamics for FOWT, Based on the MoWiT Library. *Energies*. **13** (2020), https://www.mdpi.com/1996-1073/13/8/1974

[8] Popko, W., Huhn, M., Robertson, A., Jonkman, J., Wendt, F., Müller, K., Kretschmer, M., Vorpahl, F., Hagen, T., Galinos, C. & Others Verification of a numerical model of the offshore wind turbine from the alpha ventus wind farm within oc5 phase iii. *International Conference On Offshore Mechanics And Arctic Engineering*. **51319** pp. V010T09A056 (2018)

[9] Popko, W., Robertson, A., Jonkman, J., Wendt, F., Thomas, P., Müller, K., Kretschmer, M., Ruud Hagen, T., Galinos, C., Le Dreff, J. & Others Validation of numerical models of the offshore wind turbine from the alpha ventus wind farm against full-scale measurements within OC5 phase III. *International Conference On Offshore Mechanics And Arctic Engineering*. **58899** pp. V010T09A065 (2019)

[10] Johnson, K., Pao, L., Balas, M. & Fingersh, L. Control of variable-speed wind turbines: standard and adaptive techniques for maximizing energy capture. *IEEE Control Systems Magazine*. **26**, 70-81 (2006)

[11] Jonkman, J., Butterfield, S., Musial, W. & Scott, G. Definition of a 5-MW Reference Wind Turbine for Offshore System Development. (National Renewable Eenergy Laboratory,2009)

[12] Abbas, N., Wright, A. & Pao, L. An update to the national renewable energy laboratory baseline wind turbine controller. *Journal Of Physics: Conference Series*. **1452** pp. 012002 (2020)

[13] Jafarnejadsani, H. & Pieper, J. Gain-Scheduled l1-Optimal Control of Variable-Speed-Variable-Pitch Wind Turbines. *IEEE Transactions On Control Systems Technology*. **23**, 372-379 (2014)

[14] Geyler, M. & Caselitz, P. Robust Multivariable Pitch Control Design for Load Reduction on Large Wind Turbines. *Journal Of Solar Energy Engineering*. **130** (2008,7), https://doi.org/10.1115/1.2931510, 031014

[15] Hawkins, T., White, W., Hu, G. & Sahneh, F. Wind turbine power capture control with robust estimation. *Dynamic Systems And Control Conference*. **44182** pp. 895-902 (2010)

[16] Boukhezzar, B., Siguerdidjane, H. & Hand, M. Nonlinear Control of Variable-Speed Wind Turbines for Generator Torque Limiting and Power Optimization. *Journal Of Solar Energy Engineering*. **128**, 516-530 (2006,8), https://doi.org/10.1115/1.2356496

[17] Laks, J., Pao, L., Wright, A., Kelley, N. & Jonkman, B. Blade pitch control with preview wind measurements. *48th AIAA Aerospace Sciences Meeting Including The New Horizons Forum And Aerospace Exposition*. pp. 251 (2010)

[18] Verwaal, N., Veen, G. & Wingerden, J. Predictive control of an experimental wind turbine using preview wind speed measurements. *Wind Energy*. **18**, 385-398 (2015), https://onlinelibrary.wiley.com/doi/abs/10.1002/we.1702

[19] Reiner, M. & Zimmer, D. Object-oriented modelling of wind turbines and its application for control design based on nonlinear dynamic inversion. *Mathematical And Computer Modelling Of Dynamical Systems*. **23**, 319-340 (2017), https://doi.org/10.1080/13873954.2017.1298627

[20] NREL A Reference Open Source Controller for Wind Turbines. (https://github.com/NREL/ROSCO, Accessed March 22, 2022)

[21] Semrau, G., Rimkus, S. & Das, T. Nonlinear Systems Analysis and Control of Variable Speed Wind Turbines for Multiregime Operation. *Journal Of Dynamic Systems, Measurement, And Control*. **137** (2015,4), https://doi.org/10.1115/1.4028775, 041007

[22] Jonkman, B., Mudafort, R. M., Platt, A., Branlard, E., Sprague, M., Jonkman, J., Hayman, G., Vijayakumar, G., Buhl, M., Ross, H., Bortolotti, P., Masciola, M., Ananthan, S., Schmidt, M. J., Rood, J., Mendoza, N., Hai, S. L., Hall, M., Sharma, A., Shaler, K.,

Bendl, K., Schuenemann, P., Sakievich, P., Quon, E.W., Phillips, M. R., Kusouno, N., Gonzalez Salcedo, A., Martinez, T., and Corniglion, R. OpenFAST/openfast: OpenFAST v3.1.0. (https://doi.org/10.5281/zenodo.6324288, Accessed September 08, 2022,2022)

[23] National Renewable Energy Laboratory (NREL) The FOCAL EXPERIMENTAL PROGRAM - Floating Offshore-wind and Controls Advanced Laboratory Experiment to Generate Data Set to Accelerate Innovation in Floating Wind Turbine Design and Controls. (https://arpa-e.energy.gov/technologies/projects/focal-experimental-program-floating-offshore-wind-and-controls-advanced, Accessed June 01, 2022,2020)

[24] Mendoza, N., Robertson, A., Wright, A., Jonkman, J., Wang, L., Bergua, R., Ngo, T., Das, T., Odeh, M., Mohsin, K. & Others Verification and Validation of Model-Scale Turbine Performance and Control Strategies for the IEA Wind 15 MW Reference Wind Turbine. *Energies*. **15**, 7649 (2022)

[25] Odeh, M., Mohsin, K., Ngo, T., Zalkind, D., Jonkman, J., Wright, A., Robertson, A. & Das, T. Development of a wind turbine model and simulation platform using an acausal approach: Multiphysics modeling, validation, and control. *Wind Energy*. **26**, 985-1011 (2023), https://onlinelibrary.wiley.com/doi/abs/10.1002/we.2853

[26] Mohsin, K., Odeh, M., Ngo, T. & Das, T. Causality-Free Modeling of a Wind Turbine with Open-loop and Closed-loop Validation Results. *IFAC-PapersOnLine*. **55**, 86-91 (2022), https://www.sciencedirect.com/science/article/pii/S2405896322028099, 2nd Modeling, Estimation and Control Conference MECC 2022

[27] Mohsin, K., Odeh, M., Ngo, T. & Das, T. Load Reduction of Wind Turbines Using Integrated Torque, Collective Pitch, and Individual Pitch Control Actions*. *2023 American Control Conference (ACC)*. pp. 1505-1510 (2023)

[28] Modelica Association Modelica Language. (https://modelica.org/modelicalanguage.html, Accessed January 23, 2022,2021)

[29] Tiller, M. Introduction to physical modeling with Modelica. (Springer Science Business Media,2001)

[30] Gaertner, E., Rinker, J., Sethuraman, L., Zahle, F., Anderson, B., Barter, G., Abbas, N., Meng, F., Bortolotti, P., Skrzypinski, W., Scott, G., Feil, R., Bredmose, H., Dykes, K., Shields, M., Allen, C. & Viselli, A. IEA Wind TCP Task 37: Definition of the IEA 15-Megawatt Offshore Reference Wind Turbine. (National Renewable Eenergy Laboratory,2020)

[31] Modelica Association Project Modelica Standard Library. (https://doc.modelica.org/om/Modelica.html, Accessed June 10, 2022)

[32] Greenwood, D. Principles of dynamics. (Englewood Cliffs, NJ: Prentice-Hall,1988)

[33] Ning, A., Hayman, G., Damiani, R. & Jonkman, J. Development and validation of a new blade element momentum skewed-wake model within AeroDyn. (33rd Wind Energy Symposium,2015)

[34] Jonkman, J., Hayman, G., Jonkman, B., Damiani, R. & Murray, R. AeroDyn v15 user's guide and theory manual. *NREL Draft Report*. pp. 46 (2015)

[35] Modelica Association Project Specification of the Functional Mock-Up Interface (FMI). (https://github.com/modelica/fmi-standard, Accessed March 23, 2022)

[36] Semrau, G., Rimkus, S. & Das, T. Nonlinear Systems Analysis and Control of Variable Speed Wind Turbines for Multiregime Operation. *Journal Of Dynamic Systems, Measurement, And Control*. **137** (2015,4), https://doi.org/10.1115/1.4028775, 041007

[37] Lara, K. pexels. https://www.pexels.com/search/wind

[38] Anik, B., Islam, Z. & Abdel-Aty, M. inTformer: A Time-Embedded Attention-Based Transformer for Crash Likelihood Prediction at Intersections Using Connected Vehicle Data. *ArXiv Preprint ArXiv:2307.03854*. (2023)

[39] Ahmed, P., Amin, M. & Ali, M. Leidenfrost Phenomenon and its Impact on Sessile Drop Evaporation for Different Liquids and Surfaces. (2019,11), https://doi.org/10.1115/IMECE2019-11000

[40] Song, Y., Dhinakaran, B. & Bao, X. Variable speed control of wind turbines using nonlinear and adaptive algorithms. *Journal Of Wind Engineering And Industrial Aerodynamics*. **85**, 293-308 (2000), https://www.sciencedirect.com/science/article/pii/S0167610599001312

[41] Jena, D. & Rajendran, S. A review of estimation of effective wind speed based control of wind turbines. *Renewable And Sustainable Energy Reviews*. **43** pp. 1046-1062 (2015), https://www.sciencedirect.com/science/article/pii/S1364032114010351

[42] Wang, L., Bergua, R., Robertson, A., Jonkman, J., Ngo, T., Das, T., Sarker, D., Flavia, F., Harries, R., Fowler, M., Lenfest, E., Muro, J., Burlion, L. & Bilgen, O. Experimental Validation of Models of a Hull-Based Tuned Mass Damper System for a Semisubmersible Floating Offshore Wind Turbine Platform. *Journal Of Physics: Conference Series*. **2626**, 012067 (2023,10), https://dx.doi.org/10.1088/1742-6596/2626/1/012067

[43] Li, D., Cai, W., Li, P., Jia, Z., Chen, H. & Song, Y. Neuroadaptive Variable Speed Control of Wind Turbine With Wind Speed Estimation. *IEEE Transactions On Industrial Electronics*. **63**, 7754-7764 (2016)